GEOS 2 IDENTIFICATION OF RAPIDLY MOVING CURRENT STRUCTURES IN THE EQUATORIAL OUTER MAGNETOSPHERE DURING SUBSTORMS

Patrick Robert, Roger Gendrin, Sylvaine Perraut, and Alain Roux

Centre de Recherches en Physique de l'Environnement Terrestre et Planétaire Centre National d'Etudes des Télécommunications

Arne Pedersen

Space Science Department, European Space Research and Technology Center

Abstract. The ULF magnetic and the dc electric antennas operating onboard GEOS have been used to study the origin and characteristics of short irregular pulsations (SIP's). Strong SIP's are always observed during substorm "onsets", which are characterized by an abrupt change of the GEOS dc magnetic field from a taillike configuration to a more dipolar one and which is known to be associated with rapid poleward displacement of aurorals forms in the vicinity of the GEOS field line. By applying to the three-component ULF signal a complex processing it is possible to demonstrate that most of SIP's are in fact the magnetic signatures of localized current structures passing by the spacecraft at a high velocity. Very intense spikes in the electric field (E $\simeq 3-25$ mV/m) are observed in connection with the passing over of such structures at the satellite location, but these E field spikes are generally observed 10-20 s earlier than the SIP's. On the average the E field direction is earthward with a smaller component towards cusk. Provided that the duration of the magnetic signature of the signal (2τ) is short enough (less than 2 s) it is possible to show that they correspond to field aligned current tubes (FACT's) passing by the spacecraft. When $2\tau > 2$ s, the signature of the SIP is still consistent with that of a field-aligned current tube, but this cannot be assessed without ambiguity from the ULF experiment alone. Nevertheless, the direction of the velocity of the moving structure can still be deduced from the magnetic signature. For structures detected during substorm onsets this direction is consistent (within 40°) with the drift velocity direction as determined by \underline{E} x \underline{B} . This situation occurs for 28 events out of a total of 42, which were analyzed in detail. For these events, and assuming that the amplitude of the velocity is given by $\underline{E} \times \underline{B}/B^2$, it is possible to compute the characteristic parameters of the structure: current density J, radius R (by assuming a cyclindrical structure for simplification), and velocity v. The parameters that have thus been obtained are $6.10^{-9} < J < 3.10^{-7}$ A/m^2 , 20 < R < 900 km, 15 < v < 170 km/s, with the following average values: 8×10^{-8} A/m², 215 km, and 70 km/s. When transposed to ionospheric altitudes these values are consistent with those found for localized field-aligned current structures by ground or low orbiting spacecraft observations. The origin and nature of these localized current structures are discussed. A simple theory based on the MHD stability of a field-aligned current structure is proposed to explain why the current

Copyright 1984 by the American Geophysical Union.

Paper number 3A1791. 0148-0227/84/003A-1791\$05.00

density can hardly exceed in the equatorial plane a critical value that is of the order of 10^{-7} A/m².

Introduction

The short irregular pulsations (SIP) that are often detected on the ground by ULF coils in the auroral or subauroral zones have never received a satisfactory interpretation. These ULF emissions are of an impulsive nature, and they cover a wide frequency range from 0 to above ≈ 3 Hz. They occur in conjunction with auroral activity and preferentially at the beginning of large negative bays. Contrary to other types of pulsations detected in the same frequency range such as Pc 1's or IPDP's, they were found to be associated with electron precipitation and not with fluctuations of the energetic proton distribution function [Gendrin, 1970, and references therein]. Clearly, in situ measurements in space should help understanding the origin of these emissions. Until recently, such measurements were not available because of the lack of sensitivity of onboard magnetic antennas in this frequency range. However, the payload of the European GEOS spacecraft [Knott, 1975] has overcome this difficulty, since it contains a very sensitive ULF fluxmeter that is part of an extensive field and wave experiment [S-300 Experimenters, 1979].

The first results obtained in conjunction with the observation of SIP's in space was that strong emissions occurred at substorm onsets, as evidenced on the one hand by large variations in the plasma parameters (particle injection, magnetic field change from a taillike to a dipolar configuration) and on the other hand by fast poleward displacement of the auroral forms as viewed by a system of ground all-sky cameras and photometers installed in Scandinavia in an area conjugated to GEOS [Shepherd et al., 1980].

The thorough analysis of similar events occurring either at the substorm onset or during the whole sequence of events that constitute a substorm is the subject of the present paper. However, the idea soon arose that, apart from the manifestations of an electromagnetic turbulence generated at some distance from the spacecraft, SIP's could also contain the Fourier signature of magnetic field generated by field-aligned dc currents passing by the satellite at high velocity.

Magnetospheric currents are known to be a permanent feature of the magnetosphere-ionosphere system. Such currents have been detected mainly onboard rockets [e.g., Casserly and Cloutier, 1975], onboard low-altitude polar orbiting satellites [e.g., Zmuda et al., 1970; Iijima and Potemra, 1976, 1978; Potemra, 1979] but also on higher altitude magnetospheric spacecraft such as OGO 5, IMP 4, ISEE

[Aubry et al., 1972; Fairfield, 1973; Iijima, 1974; McPherron et al., 1975; Mozer et al., 1979; McPherron and Barfield, 1980; Frank et al., 1981]. Most of the reported events are interpreted in terms of current sheets whose dimension in one direction (longitude) is large in comparison with the other (latitude). At ionospheric levels the reported current densities are of the order of a few $\mu A/m^2$ (a few nA/m^2 for those observed in the magnetotail) and their thickness is rather large (hundreds of kilometers at ionospheric levels and a fraction of an earth radius in the magnetotail).

However, some recent measurements have shown that field-aligned currents with more localized structures and larger intensities could exist along auroral field lines. These conclusions were arrived at by the use of chains of magnetometers [Baumjohann et al., 1981; Bösinger et al., 1981], incoherent scatter radar measurements [de la Beaujardière et al., 1977; Theile and Wilhelm, 1980]. A few number of events with current densities as large as $50 \mu A/m^2$ and thickness of the order of a few kilometers have been observed by Berko et al. [1975] around 800 km altitude with OGO 4. Two very localized events (R \simeq 2 km) with current densities equal to 45 and 135 $\mu\text{A/m}^2$ have been observed around 1300 km altitude with S3-2 [Burke et al., 1983]. The data that are presented here and that have been obtained in the equatorial plane around L = 6.6 can also be interpreted in terms of field-aligned currents with narrow structures and high current densities. When transposed to ionospheric level, the characteristics of these currents agree well with those described above.

From a theoretical point of view, the demonstration of the existence of localized currents in the magnetosphere and the measurement of their characteristics (size, current density, displacement velocity) are of utmost importance for the establishment of valid theories of magnetospheric substorms. The physical processes that operate at the very onset of a substorm are still the subject of controversies (see reviews by Kamide [1979], McPherron [1979], Stern [1979], and Rostoker [1980]. Quoting Akasofu [1979], "There are at least two proposed models to account for magnetotail phenomena during the expansive phase, the reconnection model and the current diversion model." In the current diversion model [Atkinson, 1967a, b; Boström, 1972; Akasofu, 1972, 1977, 1979], one assumes that a fraction of the dawn-dusk neutral sheet current is diverted toward the ionosphere, leading to downward fieldaligned currents in the postmidnight sector and to upward currents in the pre-midnight sector (downward and upward refer to the current direction as observed at the ionospheric level in the auroral zone). In the part of the equatorial region where the neutral sheet current has been diverted (the diversion slot), the magnetic field lines are restored to the dipolar configuration that they had before the intensification of the neutral sheet current took place. SIP's observed onboard GEOS at substorm onsets seem to fit well with this theory.

In this paper the following section 2 presents the gross characteristics of SIP's as deduced from the routine analysis of GEOS-ULF data in conjunction with substorm activity.

Then, pursuing data analysis, we discuss the complex data processing that has been applied in order to deconvolute the ULF signal, thus allowing to obtain the magnetic wave form. High resolu-

tion E field data are also presented and their connexion with SIP's is discussed (section 3). Then we compare the obtained magnetic signatures with those that would be produced by current sheets (single or double) or current tubes passing by the spacecraft at a large velocity (section 4).

The results obtained with such a method are presented in section 5. These results show that at least short duration SIP's can be interpreted in terms of localized field-aligned current tubes (FACT's) passing by the spacecraft at large velocities. Simultaneous quasi-static electric field measurements allow determination of the plasma drift ExB/B². If we assume that the current tubes drift with the plasma, all current characteristics can be deduced. Finally in section 6 we discuss the possible origin of these currents and we propose an explanation for the limitation of current density.

2. Observations

In this section, the magnetic spectral characteristics of magnetospheric SIP's are presented. In Figure 1, some of the characteristics of the December 29, 1978, event (see Shepherd et al. [1980], Figure 5) are presented. Panel A gives the spectrogram of the right-handed component of the signal recorded on the X and Y antennas (i.e., the antennas situated in the equatorial plane of the spacecraft, which is, within 1°, identical to the equatorial plane of the earth). Contrary to what has been observed previously for other ULF signals recorded in this frequency range [e.g., Young et al., 1981; Perraut et al., 1982], there is no variation of the spectral density at the Helium or the proton gyrofrequency. On panel B, the power integrated in the frequency range 0.4 - 10 Hz is presented. The power may reach values as high as 0.3 nT² in this frequency range. Panel D gives the dc magnetic field component B, θ , and φ , as deduced from the dc magnetometer experiment S-331 [Knott, 1975] and presented with the total intensity and the two polar angles in the VDH system (V: vertical; D: towards geographic east; H: towards geographic north). In panel C the component of this dc field in the XY plane is plotted as B_{\perp} (S-331). It shows that the field had a strong tailward component increasing regularly until 2237 UT, the time at which it suddenly decreased, indicative of a more dipolar configuration. The signal labelled D_X is the measure of the same component that can be obtained with the ULF experiment (S-300) by using the onboard "despin system" [S-300 Experimenters, 1979; Robert et al., 1979]. The agreement between the two curves is fairly good; this demonstrates that, with a suitable processing, one can get valuable information on the dc magnetic field with the ac antennas.

Two other examples are presented on Figure 2: the characteristics of the phenomena are very much the same. One may notice that each time the magnetic field changes from a tail like toward a more dipolar configuration (i.e., each time Dydecreases), strong SIP's associated with a current tube structure occur. Yet, they may also occur during the "growing phase" of the taillike structure or during the "expansion phase" of the substorm, as shown by the events near 2250 and 2310 (Figure 2a), respectively.

That these events are associated with a global perturbation of the magnetosphere and not with

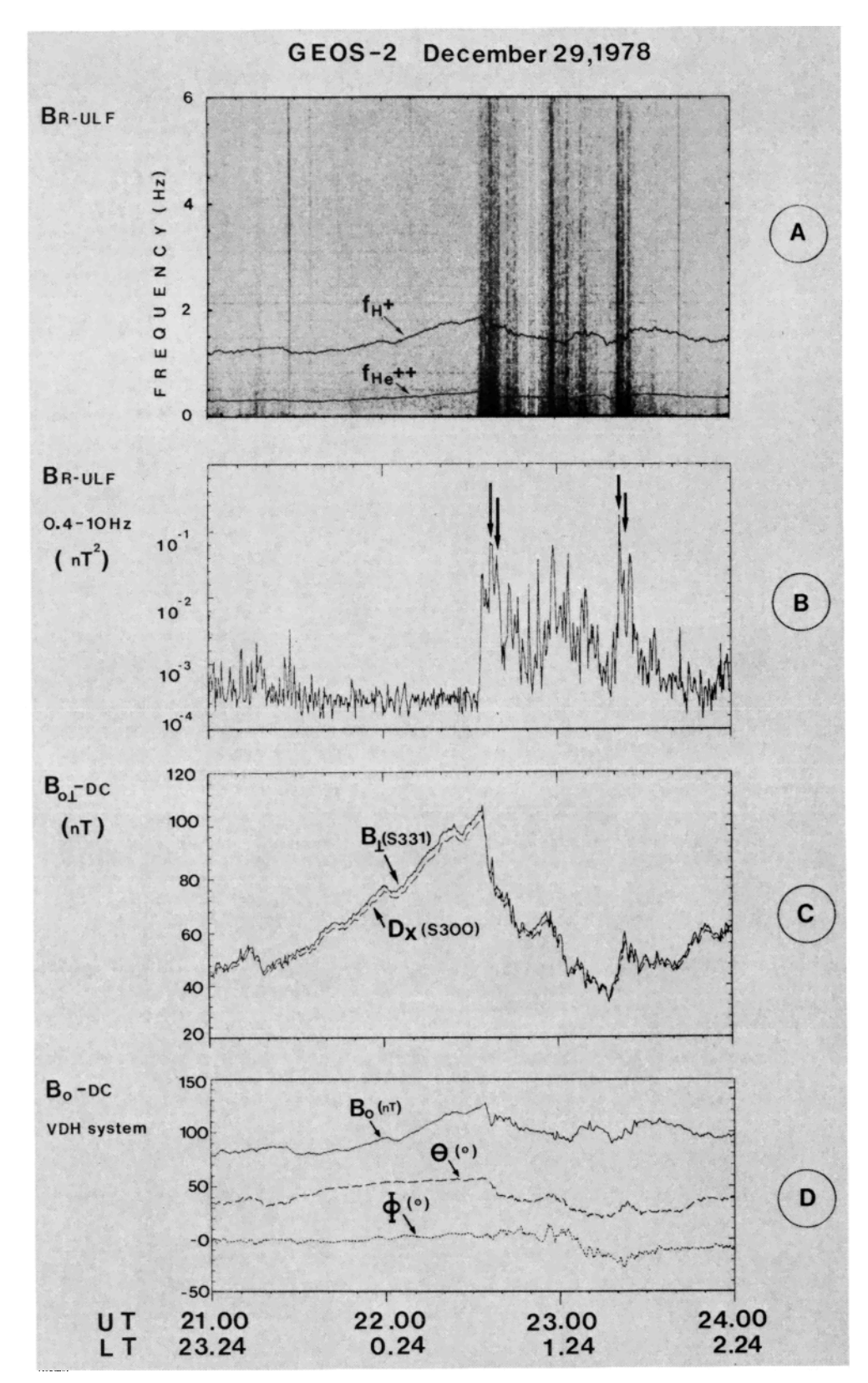


Fig. 1. Examples of SIP's observed at time of abrupt changes of the magnetic field configuration. (a) Spectrogram of the right-handed ULF component. Continuous lines represent the instantaneous helium and proton gyrofrequencies. (b) Integrated power in the frequency range 0.4-10 Hz. Arrows correspond to SIP's which have been identified as current tube signatures. (c) Amplitude of the component of the dc magnetic field in the plane perpendicular to the spin axis as obtained by two independent measurements. (d) Spherical coordinates of the dc magnetic field in the VDH system.

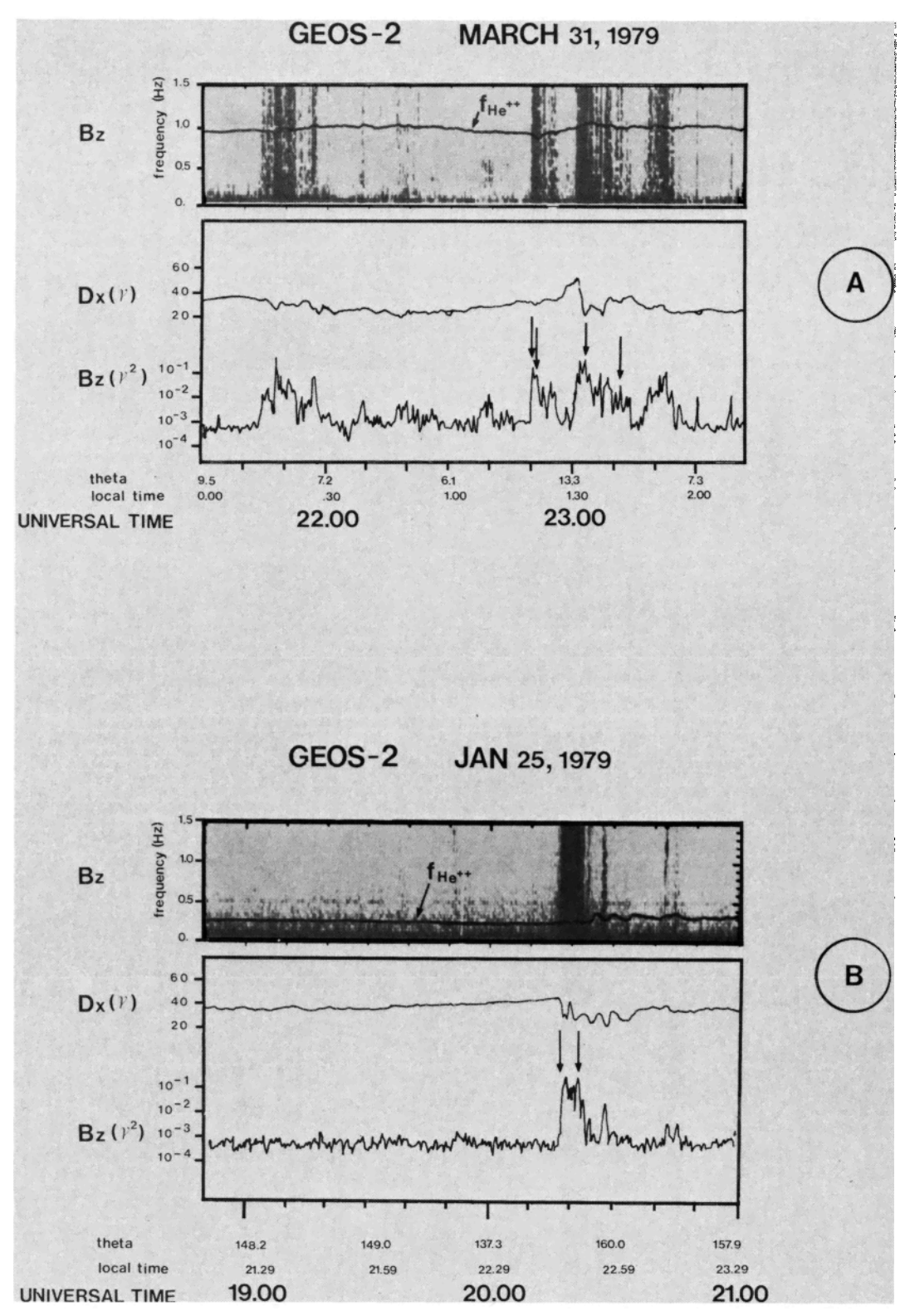


Fig. 2. Two examples of substorms associated SIP's. See Figure 1 caption for the definition of the symbols. The $\rm B_Z$ component has been plotted instead of $\rm B_R$.

a localized one is illustrated on Figure 3, where the magnetograms of three auroral stations: Kiruna (65.2°N, 116.0°E geomagnetic), Reykjavık (70°.3 N, 71.6°E), and Nassarssuaq (71.2°N, 36.8°E) are presented together with the GEOS data for a series of events that were already studied by Shepherd et al. (1980). The three auroral breakups that were detected by these authors near the GEOS magnetic footprint at 1700, 2018, and 2334 are clearly associated with substorms. Note the very pronounced tailward configuration at GEOS (B_L $\simeq 90$ nT) at least for the first two events and the large intensity of the ULF wave ($\simeq 0.3$ nT² in the frequency range 0.3-1.5 Hz and $\simeq 0.02$ nT² in the frequency range 1.5-5 Hz).

3. Data Analysis

The deconvolution method used for obtaining an equivalent dc magnetic signature is first described (section 3.1). Then the method used to obtain the electric wave form is described and compared with the magnetic signatures of current structures.

3.1. Deconvolution of the ULF Magnetic Data

The way in which the data are processed to eliminate the residue of the signal at the spin frequency and to obtain clean frequency-time spectrograms is described elsewhere [Robert et al., 1979]. For the present study we go one step further. The antennas being only sensitive to dB/dt, a correction for the frequency response must be made. Such a correction is made in the frequency domain. A fast Fourier transform is applied to a slice of signal (of 88 s duration) recorded in the spinning frame of reference. The result is multiplied by the inverse of the antenna transfer function (in both phase and amplitude). A filtering is made to eliminate the very low frequencies (f < 0.2 Hz): the antennas being not at all sensitive in this frequency range, a multiplication by the inverse of the transfer function would lead to anomalously large and not reliable numbers. A correction is also made for the delay owing to nonsimultaneous telemetry sampling of the different components. An inverse Fourier transform is then applied to come back into the time domain. Finally, the data are transposed into a fixed frame of reference (usually the VDH system) by taking into account the spacecraft attitude. The net result of this data handling is the components of B in a fixed frame of reference, within some unknown additive constant.

3.2. Example

The method is illustrated in Figure 4, which shows expanded data from a SIP event which occurred on December 29, 1978, also shown in Figure 1. At the top of Figure 4, the telemetry data corresponding to the three antennas X, Y, and Z are plotted in volts. Note that the onboard step amplifier (for the X and Y antennas alone) has switched to a lower gain between $\simeq 2321:55$ and $\simeq 2322:10$ UT so that the telemetry signal looks rather small during this period. Note also that a residual signal ($\simeq 2.5~\rm V_{pp})$ at the spin frequency is seen on both

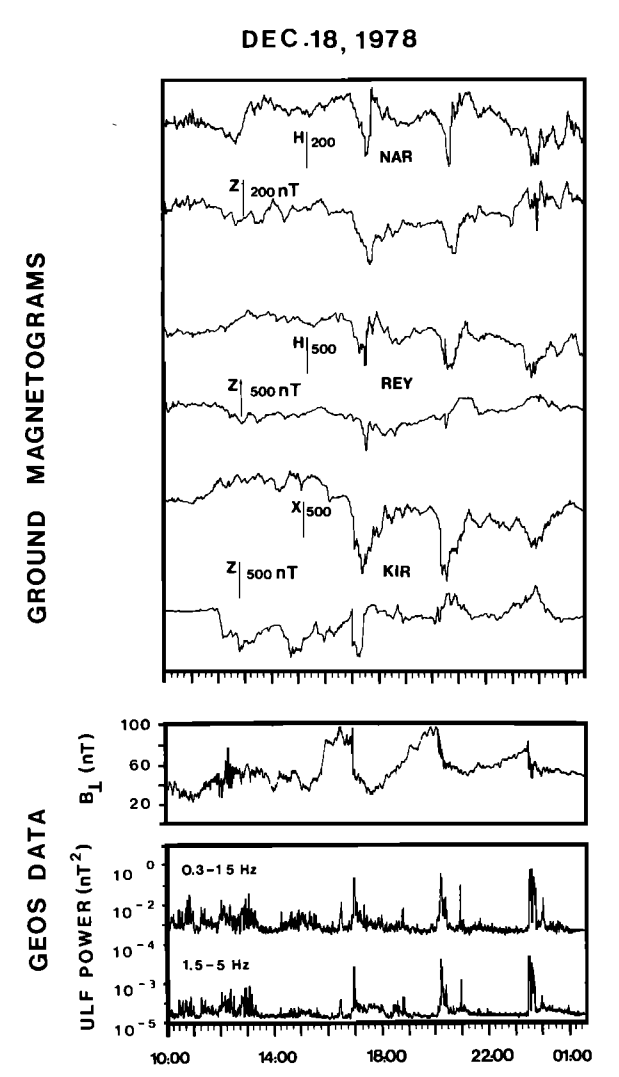


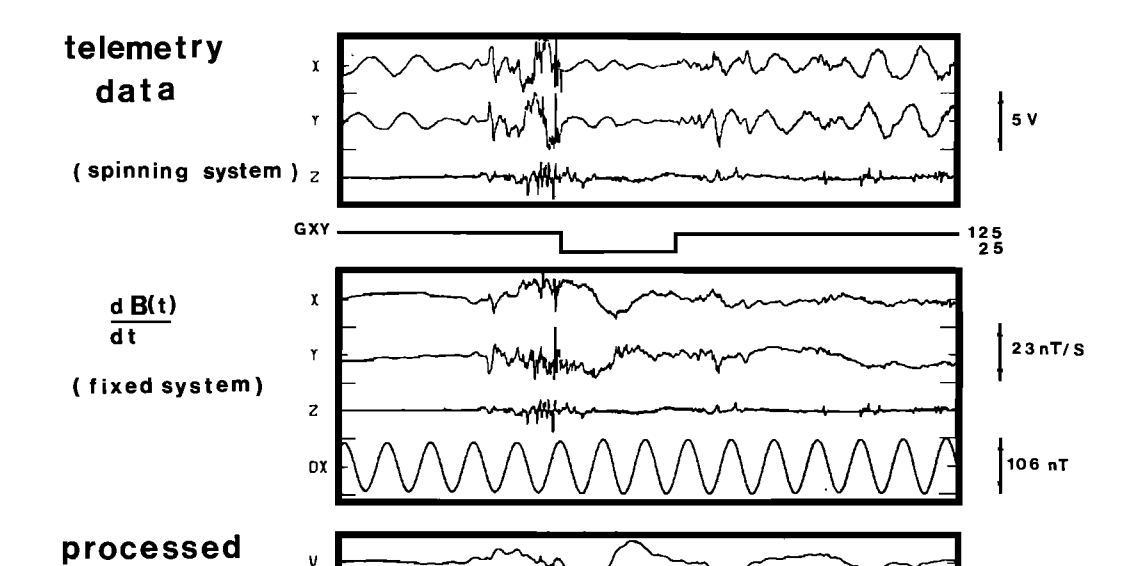
Fig. 3. The December 18, 1978, event. From top to bottom: magnetograms of Narssarsuaq, Reykjavik, and Kiruna; component of the GEOS dc magnetic field in the equatorial plane; integrated ULF power in two frequency bands showing the occurrence of SIP's at substorm "onset" times.

the X and Y antennas. In the second panel the three signals have been transformed in a fixed frame of reference and they are expressed in terms of dB/dt(nT.s $^{-1}$). A large signal with a characteristic time of 10s appears on both X and Y around 2322 UT. The signal called $D_{\rm Y}$ in this panel is the one that is transmitted independently to the ground and that serves onboard as a negative feedback to reduce the signal at the spin frequency. When converted into the same scale as the X and Y telemetered data, this would lead to an amplitude of $\simeq 35~\rm V_{pp}$, which shows the relatively good efficiency of the onboard despin system ($\simeq 25~\rm dB$). The panel below is the result of the data processing that has been described in this section.

3.3. E field Data

E field data are obtained from the electric field experiment [Pedersen et al., 1978]. The obtained high resolution wave form is plotted in Figure 5. Owing to a failure of a solar array, the electric

GEOS-2 December 29,1978



universal time

23:22:30

Fig. 4. Illustration of the data processing. From top to bottom: original telemetry signals (with an indication of the step amplifier gain); transposition to a fixed frame of reference (with the intensity of the signal induced by the rotation of the spacecraft); fully processed data; total amplitude of the magnetic signature.

23:22:00

field experiment cannot be operated on GEOS 2 during about one half of the spin period; the dotted lines on Figure 5 correspond to these time intervals where the experiment is "blind." Since the antenna is rotating at the spin frequency, the direction of the measured electric field can only be accurately determined when it varies over time scales larger than the spin period. Each arrow corresponds to the time when the antenna is oriented parallel to the earth-sun line. Then the time

data

 $B(t) + C^{te}$

(VDH system)

IB(t)I2

D

23:21:30

lag between two such arrows is the spin period. Notice the strong electric field spike at about 2321:52 UT.

11.3 nT

32.4 nT²

3.4. Combined Results

An enlarged portion of the event near 2322:00 UT is given in Figure 6, which will be described from bottom to top. The lowest panel (panel 4) represents the magnetic spectrogram of the whole

GEOS-2 December 29, 1978

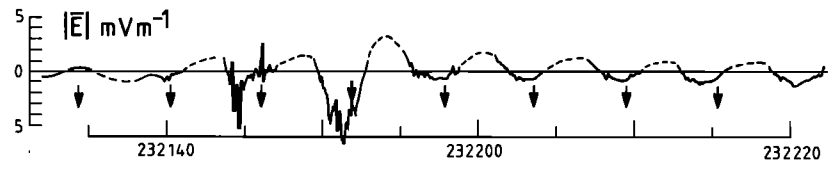


Fig. 5. Raw data output signal from the electric field double probe. Once per spin (6 s) the double probe has its closest approach to the satellite-sun line, indicated by arrows. A photoelectron effect gives rise to a sunward parasitic electric field of ≈ 1 mV m in the direction of arrows. No data is obtained for part of the spin due to a satellite solar array failure (dotted line). The large electric field, with $\approx 1-2$ Hz oscillations superimposed, seen for approximately one spin, is much larger than the parasitic sunward field.

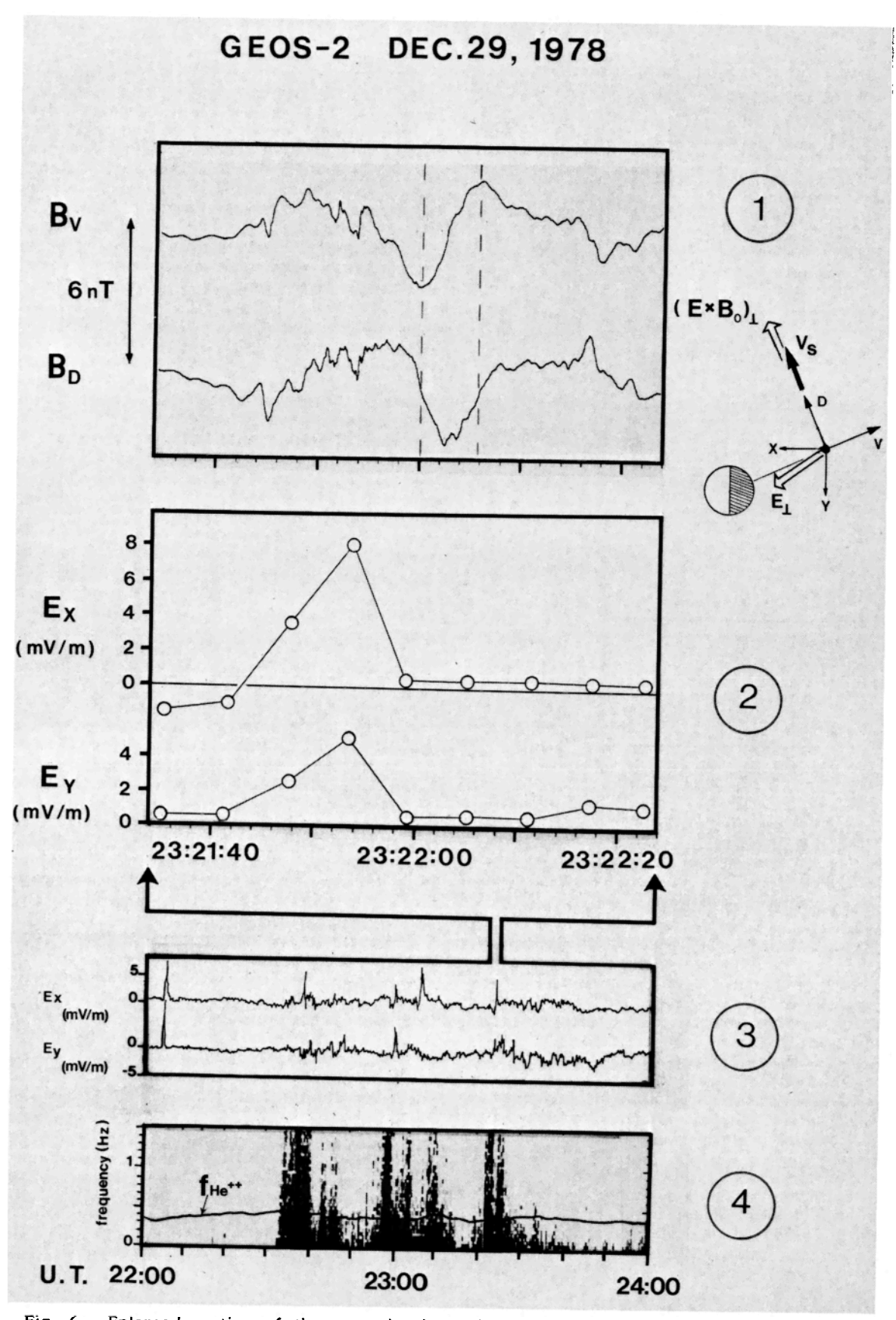


Fig. 6. Enlarged portion of the example shown in Figure 4. From top to bottom: (1) the magnetic signature in the V, D system; (2) the E field in the X-Y coordinate system, X being toward sun; each point results from an average over one spin period of data shown in Figure 5; (3) E field data and B spectrogram over 2 hours showing the general context in which the specific event under study takes place. Finally, on the right side a schematic drawing indicates both the direction of the E field and that of the direction of motion of the current structure (D).

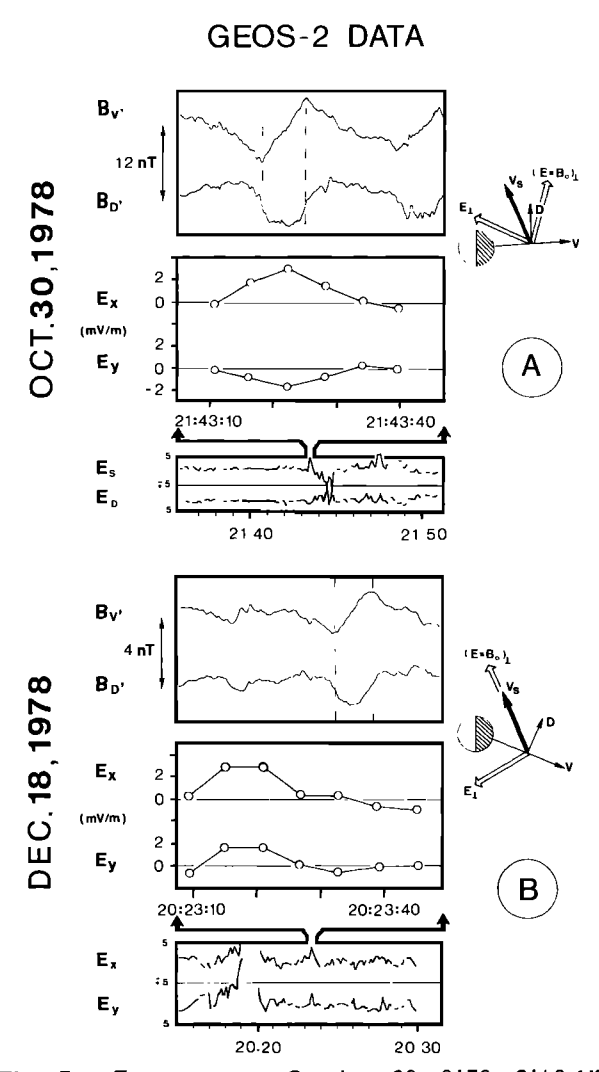


Fig. 7. Two events: October 30, 9178, 2143 UT and December 18, 1978, 2330 UT are displayed in the same format as Figure 5.

sequence of events. On panel 3 the simultaneous quasistatic electric field measurements are plotted. Ex and Ey are components of the electric field in the satellite spin plane (very close to the equatorial plane or the VD plane of the VDH system for GEOS 2). X is sunward and Y is towards dusk. Notice that large spikes ($\simeq 5$ mV m⁻¹) in the sunward component of E occur in conjunction with SIP's. On panel 2 electric field data are plotted for a selected period, spin by spin; each data point represents the averaged value (over half a spin period) of raw data displayed in Figure 5. As emphasized earlier such a procedure allows for an approximate determination of the electric field because both E_X and E_Y vary considerably from spin to spin. The error bar on both E_X and E_Y is in the range (1-2 mV m⁻¹). Panel 1 gives the magnetic signatures of two components of the magnetic wave form as deduced from the ULF experiment. This signature is characterized by different wave forms on the two components: one resembles a gaussian curve, the other resembling the derivative of a gaussian. For reasons that will be clarified later, this magnetic signature could be displayed in a D',V' system, which is deduced from a D,V system by a rotation. Indeed it will be shown in section 4 that the magnetic signature in Figure 6 corresponds to a localized current structure moving in the D direction. We further note that the E field spike is observed about 10 s before the B field spikes (which will later be shown to correspond to a current structure passing by the spacecraft location). This delay between the appearance of the E field spike and the occurrence of the magnetic signatures of current structures is apparently quite general; however, we found an exception that is displayed in Figure 7a, with the same format. In this peculiar case, the E field spike (mostly in the X direction) coincides with the magnetic signature; however, the latter lasts less than the former. Two other examples are shown in Figures 8a and 8b. In this case the electric field spike is again observed prior to the magnetic signature of the current structure.

For each of the above discussed examples we have also presented a schematic graph indicating the directions of the E field spikes together with the direction D', which will later be shown to coincide with the direction of the motion of the current structure. In four cases the E field spikes are almost sunward; in the fifth, however, the E field spike points roughly antisunward. In all cases D' is orthogonal to Esp (sp stands for spikes) and thus D' approximately coincides with the Esp x B direction; note that such a property is not trivial, since short duration E field spikes do not necessarily imply a regular E x B drift. Indeed we will show in the last section that it is different for SIP's which are not observed during substorm onsets.

As a last remark we note that the B field wave form in Figure 8a is quite complex and exhibits an intense higher frequency signal ($T \simeq 1.5 \text{ s}$) superimposed on the main signature. In addition to this presumably turbulent feature we also notice that a second, weaker and less clear current signature is observed at $\simeq 2021:17$; it is accompanied by an E field spike with a large E_{γ} component (also consistent with $V_{\gamma} \cdot E_{\gamma} = 0$). In conclusion, $V_{\gamma} \cdot E_{\gamma} = 0$.

In conclusion, we note that there seems to exist a causal relationship between strong E field spikes and the magnetic wave form during SIP's. In the following an attempt will be made to interpret these signatures.

4. Models and Comparisons With Simulated Signals

First, the magnetic signatures of a moving current sheet or double-sheet will be described and compared with the signature of a moving current tube. Then we will characterize these signatures as a function of the orientation of the velocity of the quoted structure with respect to a given frame of reference. A similar study has been undertaken earlier by Berko et al. [1975], who, however, used data acquired onboard a stabilized and low altitude satellite.

4.1. Current Sheets

Let us first consider a FAC sheet and let us assume that the spacecraft crosses this sheet along a trajectory that is orthogonal to the current (it is equivalent to consider that the sheet is moving and encounters the spacecraft). If a fixed frame

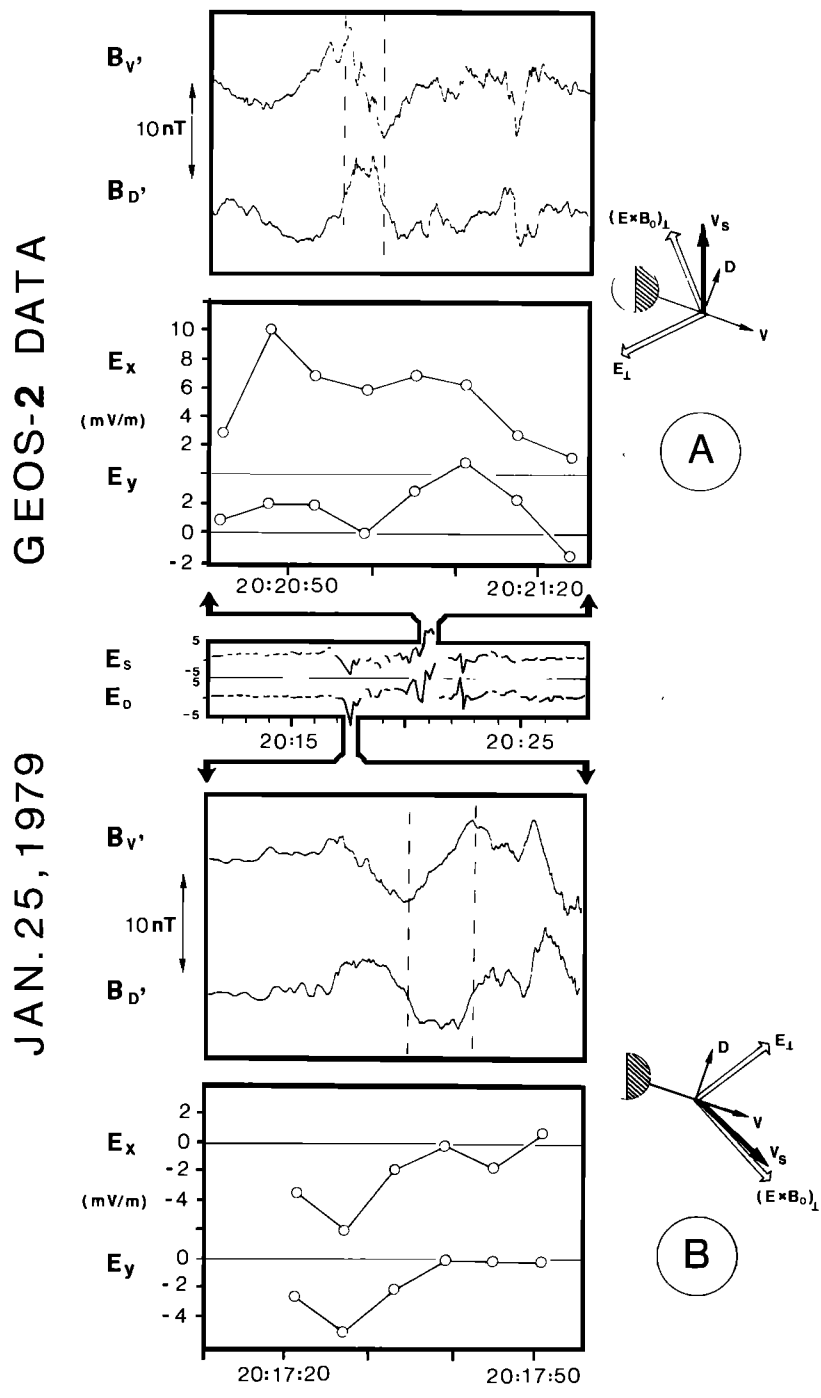


Fig. 8. Same as Figure 7 for January 25, 1979, 2021.00 and 2017.30 UT.

of reference is considered, that is if the sheet does not rotate simultaneously, it is easily found that the magnetic field signatures observed on the two antennas will be proportional to each other (Figure 9), the proportionality coefficient being either positive or negative depending on the orientation of the antennas with respect to the sheet. For reasons of simplicity, we have assumed that the antenna axes X_1 and Y_1 are oriented parallel and perpendicular to the relative trajectory of the spacecraft and the sheet, but the argument holds for any other orientation, the proportionality coefficient being possibly equal to zero for some

orientations. In the actual situation the true antennas X and Y are rotating, but with the help of some simple processing (see section 3.1) it is possible to reconstruct the signals as if they were observed in a fixed frame of reference. From now on this frame of reference will be assumed to be parallel and perpendicular to the relative motion and we will drop the subscript 1.

A point that is worth emphasizing is that magnetic wave forms, such as those displayed in Figures 6, 7, and 8, cannot result from the local enhancement (and further decrease) of a nonmoving current structure. Indeed if they were due to such

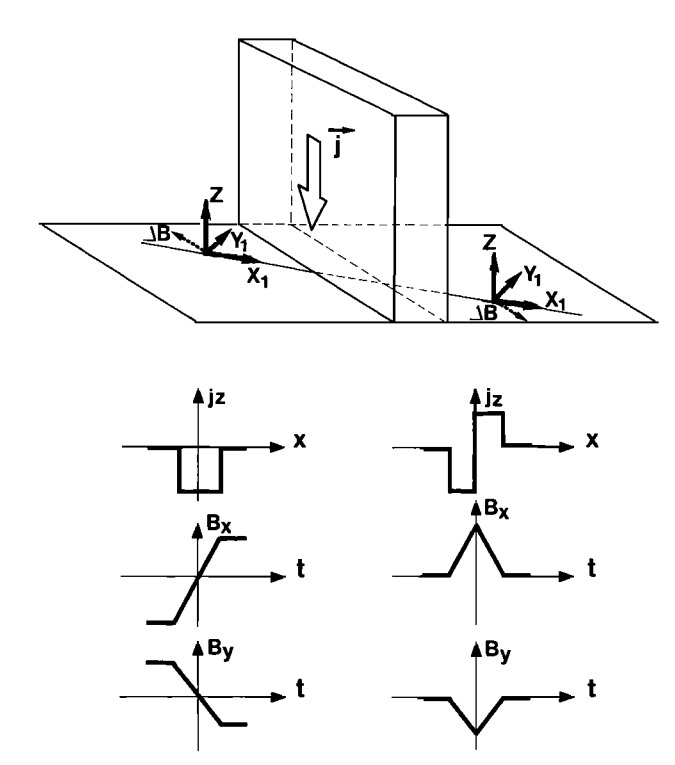


Fig. 9. Theoretical magnetic signatures recorded on two orthogonal antennas when the spacecraft crosses an infinite current sheet. In the bottom part of the figure, the signature has been represented for a single sheet (left) and for a double sheet (right).

a short-lived structure, the two magnetic components should vary in phase, a phenomenon that we do not observe in general.

4.2. Current Tubes

Let us consider now a field-aligned current tube (FACT). Two situations may occur (Figure 10). In the first one (Figure 10a), the spacecraft does not cross the tube of current. If I is the total current within the tube and if a is the impact parameter (the distance of closest approach) the curves giving the variation of B and B as a function of time are very regular, although both variations have very different shapes. At time $\tau = a/v$ (where v is the relative velocity) B goes through its maximum value B $_{V} = \mu$ I/ 4π a, whereas B has half the value it had at time = 0 (B = μ 1/ 2π a). The quantity 2τ may be considered as the characteristic time of the encounter. If one measures this characteristic time, as well as the maximum amplitudes B and B $_{V}$ 0, one must first verify that $2B_{V} = B_{X0}$ and second one obtains a measurement of I/a. The current tube and its displacement being defined by three parameters a, I, and v and the experiment giving only two measures (a/v and I/a) it is impossible to deduce from the ULF experiment alone all the characteristics of the FACT. In section 5 it will be shown that it is sometimes possible to get a third independent measurement (E field) that will allow us to obtain all the FACT characteristics.

The second situation (Figure 10b and 10c) occurs when the spacecraft crosses the current tube. Assuming that the current density J is con-

stant over the whole area $\pi\,R^2$ of the tube (and therefore that the total current intensity I is equal to $\pi\,R^2$ J), the B_X(t) and B_Y(t) curves do present angular points which occur at a time t₀, where

$$t_{0} = \tau (R^{2}/a^{2}-1)^{1/2}$$
 (1)

Depending on the relative value of a and R (a/R $\gtrsim 1/\sqrt{2}$), the shape of the B (t) curves are slightly different. In the first case, there is not much change in the slope of the curve at the angular point, whereas the slope changes sign in the second one. In both cases, assuming that we measure B $_{\rm Xmax}$, B $_{\rm Ymax}$, and τ (first case) or t (second case), it is possible to deduce the values of Ja, a/r, and a/v. Again ones does not have enough measurements for deducing all the FACT parameters, which are now four in number : a, R, J, and v. Even if we could measure t (first case) or τ (second case), this would not help because the ratio τ/t_0 is not independent from the other parameters.

4.3. Orientation Effects

One question immediately arises: how do these magnetic signatures change when the reference axes are no more parallel or perpendicular to the direction of the relative displacement? This question is easily solved by a numerical simulation in which the angle θ (made by the relative spacecraft velocity vector $\mathbf{v_c}$ with respect to the X antenna) is varied.

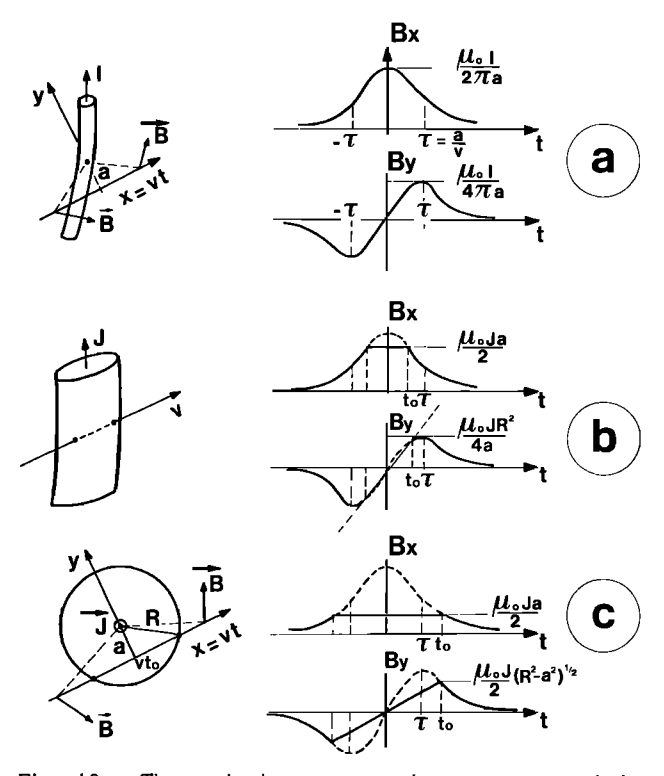


Fig. 10. Theoretical magnetic signatures recorded on two orthogonal antennas when the spacecraft passes by (a) and crosses (b and c) a field-aligned current tube. The X antenna is assumed to be oriented in the direction of the displacement. Case (a) corresponds to a > R, (b) to $1\sqrt{2}$ < a/R < 1 and (c) to a/R < $1\sqrt{2}$.

On Figure 11 the results of such a simulation are presented when θ varies from 0° to 90°. One verifies that Y(90°) is identical to X(0°), whereas X(90°) = -Y (0°) as it could be expected from simple geometrical considerations.

Similar curves may be drawn for all azimuthal angles. Fitting the experimental data with these curves may allow the determination of θ . In fact, data are processed the other way round. The dc magnetic signature is computed in different frames of reference until one finds curves that look like the θ = 0° of the θ = 90° curves. This fitting procedure is made with angular steps of 22.5°, which is the accuracy of the determination of θ .

However, one must note that there exists an ambiguity in the direction of the current. The simulation results presented in Figure 11a for instance have been obtained by assuming that the current was pointing upward, that the spacecraft was moving to the right and passing below the tube. Identical signatures would be obtained for a current pointing downward (with respect to the plane of the figure) with a spacecraft moving to the left and passing above the tube. There is no way, by using magnetic data alone, to distinguish between these two possibilities. Again we must look for an independent information (see section 5).

The simulations presented in Figure 11 have been made by assuming the following and typical values for the current parameters: $J = 7 \times 10^{-8}$ A.m⁻², R = 200 km, v = 70 km s⁻¹ and a varying between 80 and 320 km. For such parameters τ (or t₂) is of the order of 5 s and the maximum amplitude of the magnetic signal is between 1 and 10 nT.

4.4. Simulated Signals

In order to check the validity of the method, an artificial magnetic signature of a FACT has been fed through a simulated antenna system and the method has been applied to the issuing signals. The results are shown in Figure 12 for the two characteristic signatures of a moving current tube, noted B₁ and B₂. One sees that, for the spinning antennas X and Y, there is not much difference between the original input signal and the output one, filtered in the spinning frame of reference and recomputed in the original fixed referential. In particular the shapes of the signatures are much similar and the times τ or to are identical. Only a slight low frequency modulation may be noticed, which is due to the artificial suppression of frequencies smaller than 0.2 Hz. But the results are quite different on the nonspinning (Z) antenna. The amplitude of the output signal is reduced by a factor 2 or 3 and the low frequency modulation becomes of the same order of magnitude as the total signal.

All these characteristics are easily explained. Filtering at 0.2 Hz strongly attenuates signals with characteristic times longer than 5 s: this is what is observed on the Z antenna. But in the rotating frame of the X and Y antennas, a dc magnetic field with a given orientation in a fixed frame generates an ac signal at the spin frequency ($\simeq 0.17$ Hz). Filtering at 0.2 Hz is equivalent to filtering the original signal at $\simeq 0.03$ Hz and magnetic signatures with characteristic times shorter than 5 s are almost not modified.

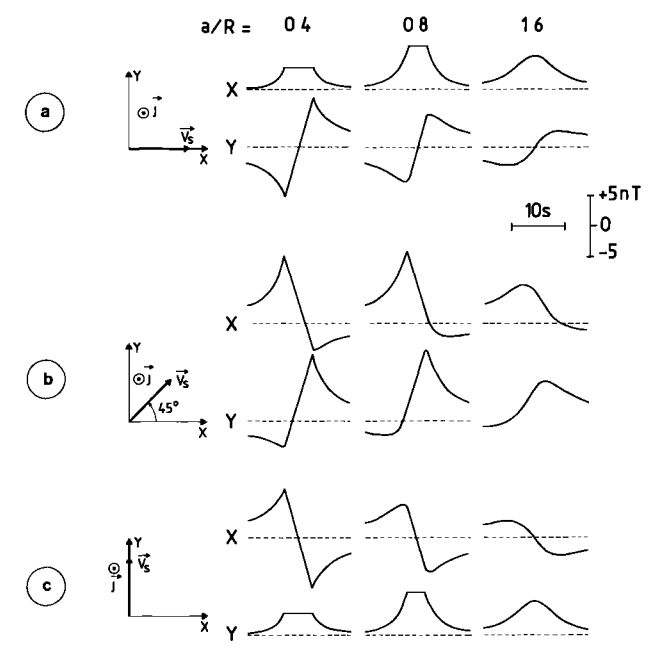


Fig. 11. Numerical simulation of the magnetic signatures that would be observed on two orthogonal antennas when the velocity of the spacecraft with respect to the current tube makes an arbitrary angle with the reference X axis. The parameters of the FACT model are R=200 km, $J=7x10^{-8} \text{ A m}^{-2}$, and $v=70 \text{ km s}^{-1}$. The impact parameter a is varied as indicated.

4.5. Method Efficiency

In order to specify the limit of the method, other simulations of FACT's have been made with different characteristic times and different values of the ratio a/R. This leads us to the determination of the transfer function of the system for the input model signals $B_1(t)$ and $B_2(t)$. The results (which will be used for deducing absolute amplitudes of the magnetic signatures) are presented in Figure 13. For the spinning antennas, the ratio between the output amplitude to the input amplitude A_0/A_1 slowly decreases when τ increases. One can expect to find magnetic signatures on the X and Y antennas for τ values as large as 10-15 s. Yet for the Z antenna that is not spinning, we cannot expect to find signatures for τ larger than 2-3 s.

Another limitation to the accuracy of the determination of the geometry of current structures must also be discussed. Owing to spacecraft rotation, the effect of the filtering at 0.2 Hz is not the same for two vectors rotating with and against the satellite spin. B field vectors rotating in the same sense as the spacecraft will be strongly attenuated, while those rotating in the opposite sense will be properly reproduced. Thus data processing has led to select a class of signatures that correspond to a counterspin rotation. Yet, because of the seasonal change of the GEOS spin direction, we have had almost equal chances to select events corresponding to apparent left- or right-handed rotation, so that the statistics of the current direction (see section 5.1.) is not basically biased. The same difficulty is also met when analyzing a linearly polarized signal, due for instance to a double current sheet with a current flowing in the Z direc-

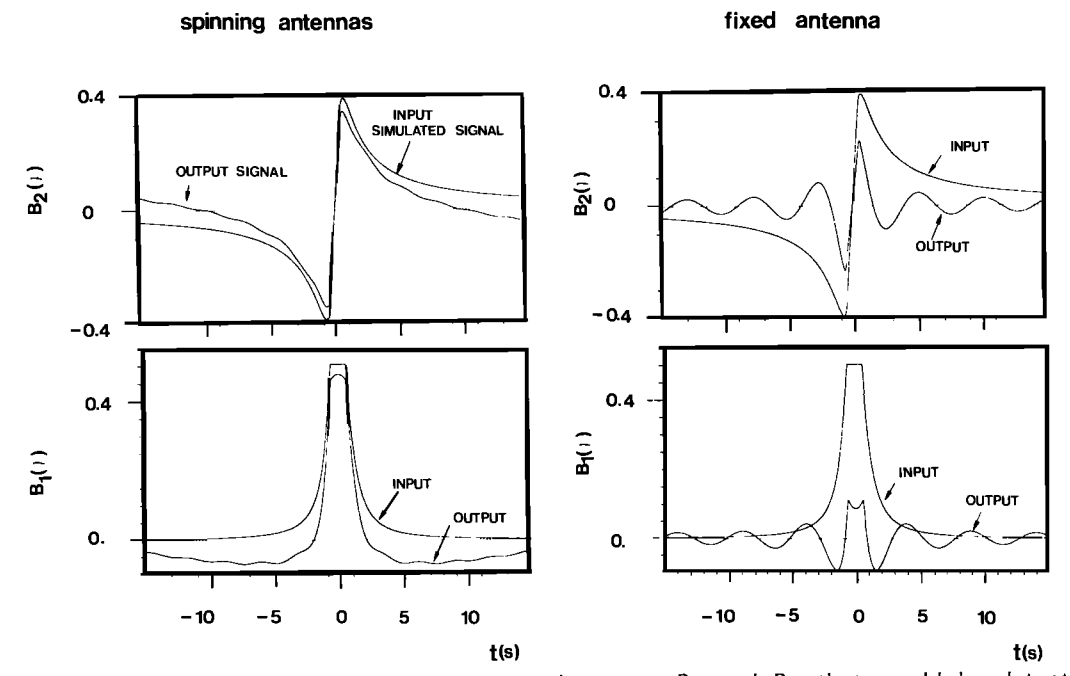


Fig. 12. Comparison between the magnetic signatures B_1 and B_2 that would be detected by truly dc magnetic antennas and the ones that are obtained after processing the AC ULF data. For the spinning antennas, oscillations occur due to the ultra-low frequency filtering. These effects are much enhanced for the nonspinning antenna. The following current tube parameters were assumed: R = 100 km, a = 80 km, a = 100 km, a

tion. Then it is found from simulations that a parasitic signal is introduced in a direction perpendicular to the original one. These parasitic effects, of course, depend upon the duration of the signature. After a careful study of these effects upon simulated signals we can conclude that the field-aligned current tube geometry can only be assessed without ambiguity when the signatures last less than 2 s. As a matter of fact, magnetic signatures such as those displayed in Figures 6, 7, and 8, which are consistent with FACT's, might also be due to a double sheet structure passing the spacecraft.

Nevertheless, an important remark is in order: when after a suitable rotation of the magnetic signature in the X-Y plane we get a single humped component in one (and only one) direction, say D', we can be sure that the structure (whatever its cross section in the spin plane might be, circular elliptical, banded) moves in the D' direction. This property will be used in section 5 where we compare the direction of motion of these structures with the $\underline{E} \times \underline{B}$ drift.

4.6. Examples of FACT's

In order to assess without any ambiguity the geometry of the current structures that have been detected on GEOS, we have selected magnetic signatures lasting less than 2 s. Our Figure 14 shows such a signature. In Figure 14a a rotation has been made in the spin plane (VDH \rightarrow V'D'H') so as to obtain the best fit with the theoretical signature of a tube. In Figure 14b we go one step further; in order to prove that the current flows along B we have changed (V'D'H') \rightarrow (X'Y'B) where X is in the plane defined by V' and B and is perpendicular to B. It is clear in Figure 14b that the component along B is now much smaller

than the other two components (while the H component is approximately as large as the V' and D' components). We thus conclude that the magnetic signature is that of a field-aligned current tube.

Another such example is displayed in Figure 15. In this case a rotation in the VD plane is not useful since the D component already exhibits a single humped variation while the V component

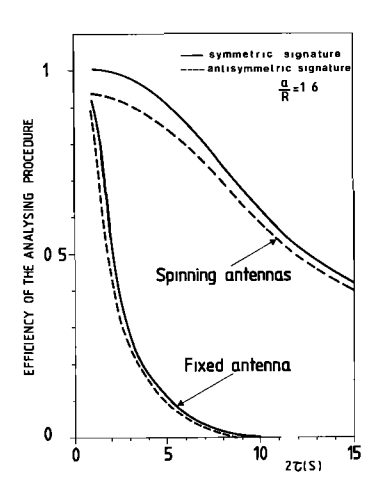
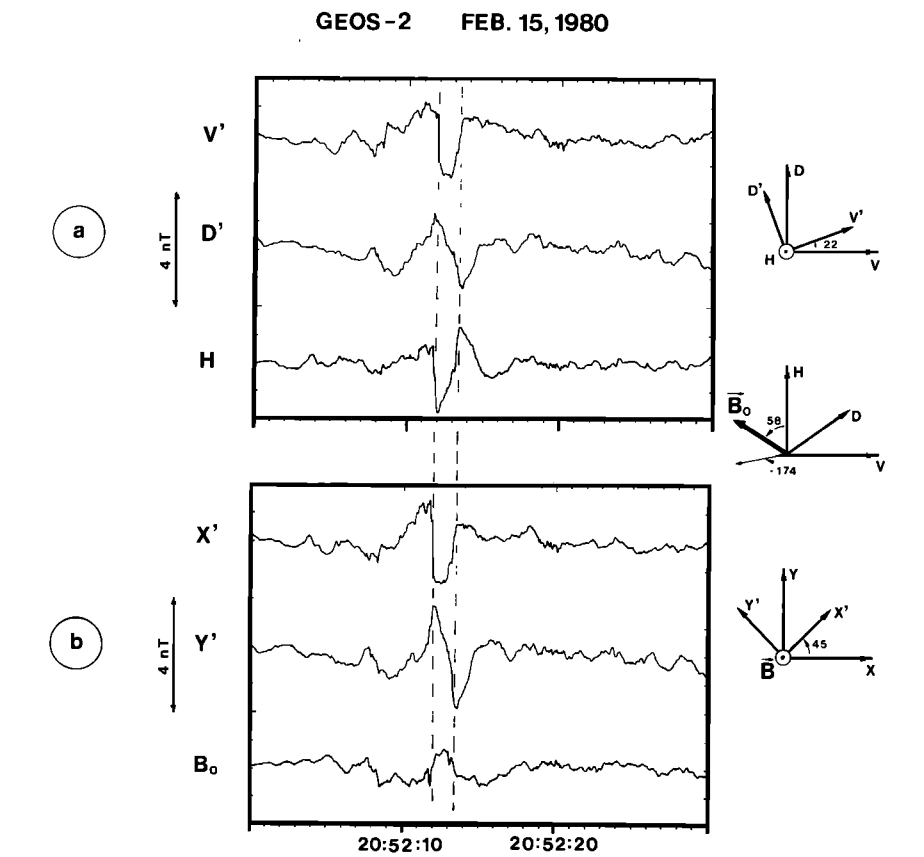


Fig. 13. Efficiency of the analyzing procedure as a function of the characteristic time 2τ of the magnetic signature. I and 2 refer to the nature of the signature (symmetric or antisymmetric) as represented in Figure 12. The efficiency of the nonspinning antenna is much reduced as soon as the characteristic time of the signature exceeds 2 s. There is also a slight influence of the ratio between the impact parameter a and the radius R of the current tube (not shown here).



Detection of a field-aligned current tube. Since the characteristic time of the event is rather short ($2\tau \simeq 1.6$ s), there is a magnetic signature on the three antennas and therefore on the three directions V', D', and H (upper panel). When transposed to a frame of reference in which the Z axis is parallel to B, the signature along this axis almost disappears (lower panel), which is a proof that the current flows along B; at that time the angle between B, and H was 58°.

has a double-humped type signature. Note that the H component is as large as the other; yet, once in the (X,Y,B) plane (Figure 15b) the component along \underline{B} becomes very small, as expected for the signature of a current flowing along \underline{B} . We thus conclude that we are observing a FACT moving in the \underline{D} (or $\underline{-D}$) direction.

Seven such events have been identified among the 47 events studied in detail. The remaining 40 events last more than the critical value of 2 s, which makes it difficult to assess whether they are also FACT's. Such a check requires high time resolution data from the fluxgate magnetometer, a task that will be the object of a future work.

5. Statistical Results

Because of their huge number, we have not made a systematic analysis of all SIP's, which have been observed onboard GEOS 2. We have selected in priority those SIP's for which magnetic signatures were clear. This is not always the case : often a "turbulent" magnetic field is superimposed on the current signature. This is illustrated in Figure 8a, where such a superposition is observed at the beginning of the signature. In this particular case, as in many others, both contributions can easily be separated. However, the turbulent field

can have an amplitude comparable to that of the current signature. In such cases it is difficult to analyze the geometry of the structure; in our selection we have deleted these events.

Looking at intense onsets, we always found simultaneous SIP's. However, electric field measurements were not always available at these onset times. Because the knowledge of this field is necessary to compute all the current parameters, as will now be discussed, we have also looked at SIP's near substorm onsets when electric field data could be obtained. A total of 42 cases have been analysed by using the method described in the previous Section.

5.1. Velocity of Current Structures

As discussed at the end of section 4, whatever is the duration of a magnetic structure, as measured from its wave form, it is possible to derive from it the direction of its motion. A series of rotation (22,5° - 45° - 67.5°) has been applied to the two components of the wave form in the spin plane; whenever the resulting signatures exhibit a single and double humped function, the one corresponding to the single humped is the direction of the displacement. We will now compare this direction to the one given by $\underline{v} = (\underline{E} \times \underline{B}_0)/B_0^2$.

Partial results of such oa comparison have

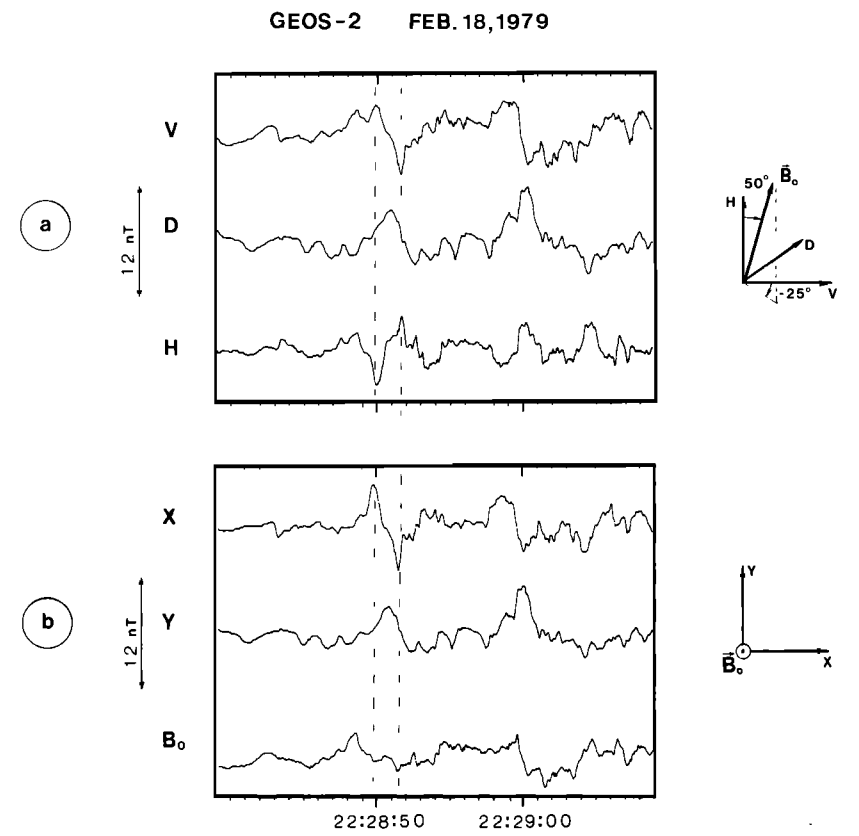


Fig. 15. Another example of a field-aligned current tube. At that time the angle between $B_{\rm o}$ and H was 50°.

already been shown in Figures 6, 7, and 8, where we found that \underline{v} , the motion direction of the signature, is perpendicular to \underline{E} sp (remember, however, that there is generally a time lag between both, as emphasized in section 3). We thus conclude from data shown in these figures that the projection of \underline{v} and $\underline{v} = \underline{E} \times \underline{B} / B$ in the spin plane coincides. As will now be discussed, this is not general; indeed statistics made on the basis of 42 current signatures analyzed in detail and compared with the corresponding high resolution \underline{E} field data show two different trends. Observe that \underline{v} is defined modulo 180° ; therefore, we have chosen in what follows the direction of the current and \underline{v} so that the angle $\Delta \varphi = (\underline{v}, \underline{v})$ be minimized. It appears that there are cases for which the agreement between the two directions is rather good ($|\Delta \varphi| \leq 30^\circ$) and cases for which it is not.

The comparison between the orientation of \underline{v} and $\underline{-v}$ is made in Figure 16, where we have separated cases corresponding to substorm onsets as defined in section 2 (i.e., current structures observed at a time of abrupt changes of the magnetic field configuration), from cases corresponding to other periods within a substorm. The first class of events is characterized by the symbol $D_{\overline{A}}$ (and contains 14 events observed during 7 different days). The second one (28 events during 8 different days) is characterized by the symbol $D_{\overline{A}}$.

Examination of the first class shows that

Examination of the first class shows that the agreement between \underline{v} and $\underline{-v}$ is rather good: out of the 14 cases, nine correspond to $|\Delta \varphi| \leq 20^{\circ}$) and all to $|\Delta \varphi| \leq 40^{\circ}$. Observe that \underline{v} is at best determined within \simeq 11° and \underline{v} within \simeq 20°

- 40° (whereas the accuracy on the measurement of |v| is \simeq 20%). These accuracies are still good enough to allow to conclude that for these events, the displacement of the current tube is imposed by the $E \times B$ drift. This solves the ambiguity problem about the direction of the current (upward or downward). Accordingly, assuming that $v = E \times B$ /B gives us the last missing parameter for computing current characteristics. Examination of the panels corresponding to this class of events also shows that within three exceptions, the general direction of the $E \times B$ drift is eastward with a slight component oriented earthward. In other words the plasma (and the current tubes) follow the direction of newly injected electrons.

For the second class of events the situation is less clear. Only 8 events out of 28 correspond to $|\Delta \varphi| \leq 20^\circ$ and 15 to $|\Delta \varphi| \leq 40^\circ$. Besides the ExB drift directions are more randomly distributed.

By using E field measurements for suppressing the ambiguity in the direction of the current, one can draw a map showing the direction of this current as a function of local time. This is done in Figure 17 for the 29 events for which $|\Delta\,\varphi\>| \le 40^{\circ}.$ In this figure the radial coordinate has no physical meaning: it is used merely to separate points. Again these events have been divided into two classes, associated or not with substorm onsets. In both classes more than half of the events correspond to currents pointing upward. In order to know whether an upward current corresponds to electrons precipitating into the ionosphere or flowing out of the ionosophere, one has to consider the relative position of GEOS with respect to the neutral sheet.

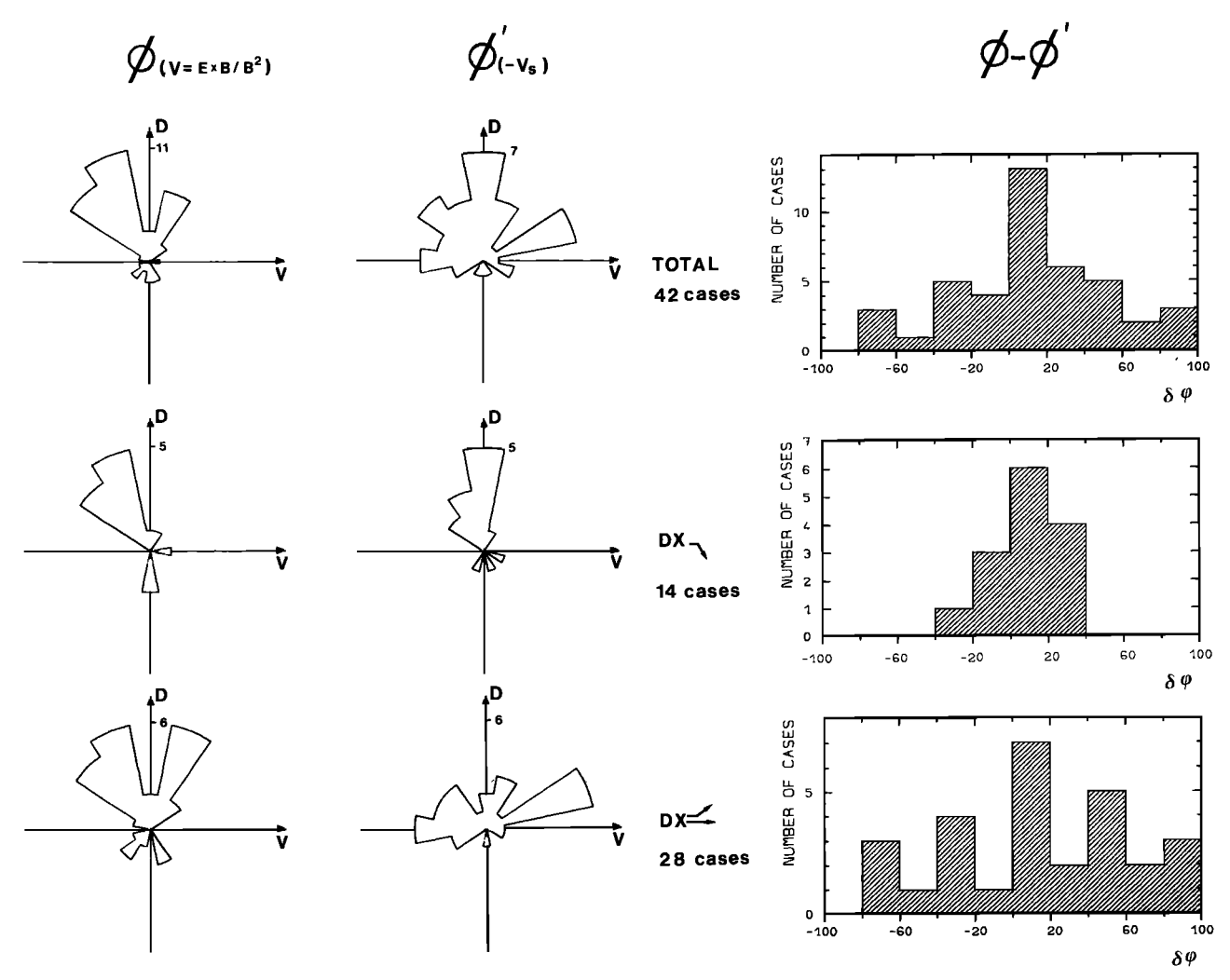


Fig. 16. Repartition, in 22.5° angular slices, of the velocity v (as deduced from E field measurements) and of the velocity -v (as deduced from the ULF magnetic signature) of the current tubes. The histograms of the angular differences of the two directions, as measured for each individual events, are also plotted (in 20° bins). From top to bottom: all events, events associated with "onsets" ($D_{\sqrt{*}}$), events non associated with "onsets" ($D_{\sqrt{*}}$). For the onset-associated events, the two directions of the velocity are much similar. In their majority they correspond to an eastward (and slightly inward) displacement of the tube.

GEOS 2 is situated in the geographic equatorial plane and a few degrees south of the magnetic equator. Indeed examination of \underline{B} polar angles in the VDH system (see Figure $\overline{180}$, where θ is the angle between H and B and φ is the angle between V and $\underline{B_1}$) shows that in almost all cases GEOS is south of the neutral sheet; i.e., the magnetic field passing through GEOS is stretched toward the tail and not toward the earth ($\varphi \simeq 0^\circ$ and not 180°). Consequently, more than half of the observed currents correspond to electrons precipitating into the southern hemisphere. However, this study should be complemented by measurements obtained at higher magnetic latitudes.

5.2. Current characteristics

For the 29 events for which $|\Delta \varphi| \le 40^\circ$, all the current characteristics have been computed. For this purpose we have assumed that all the observed signatures correspond to FACT's, an assumption that might be wrong for those lasting

more than 2 s. Nevertheless, current densities and speed of structures remain accurately determined, whatever the geometry of the current structure: if the structure consists of a sheet or double sheet (as it might be the case for long lasting signatures), the parameter R becomes an approximate evaluation of its size in the direction of the motion. The maximum, minimum, and average values of these parameters are given in Table 1, whereas their distributions are represented in Figure 19. In the next section a comparison will be made between these values and those determined onboard low altitude spacecraft or deduced from ground measurements. Notice that R is of the order of a few Larmor radii for 1-keV protons.

5.3. <u>Ionospheric equivalence</u>

The mirror ratio ρ = B₁/B₂ between the ionosphere and the equatorial region (at the geostationary orbit) is of the order of 500. Assuming that the total current within a flux tube is conserved,

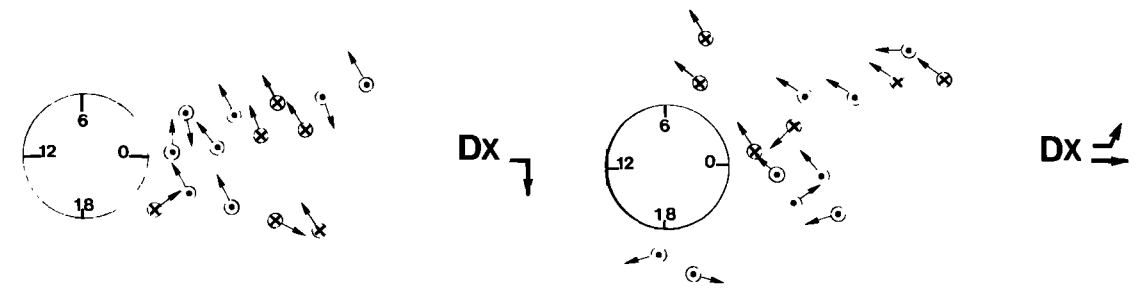


Fig. 17. Current direction and velocity (as seen from above the North Pole) for the events for which $|\Delta \varphi| \le 40^{\circ}$. The plotted velocity is the one deduced from E field measurements. The radial coordinate is just used for separating points.

one has

$$R_i/R_e = \rho^{-1/2}$$

$$J_i/J_e = \rho$$
(2)

$$(JR)_{i}/(JR)_{e} = \rho^{1/2}$$
 (3)

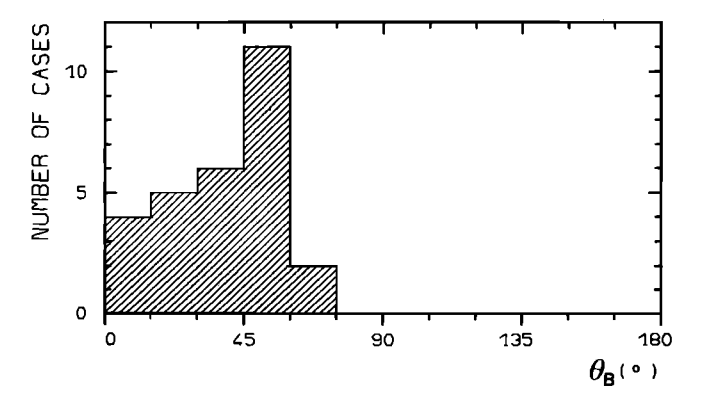
where subscripts i and e stand for the ionosphere and the equator, respectively. If we assume that the azimuthal angular yelocities are also conserved, one has $v_1/v_e \simeq 1.4 = 0.06$. From the observed equatorial values reported in the previous section, the corresponding ionospheric values are obtained (see Table 1).

Values of the order of 1 - 3 μA m⁻² are usually found with spacecraft for the global two sheets field-aligned current system [e.g., Iijima and Potemra, 1976, 1978; Potemra, 1979] but larger values (10-40 μA m⁻²) have been observed onboard rockets or spacecraft or deduced from incoherent scatter radar measurements in the vicinity of more localized auroral forms [Casserly and Cloutier, 1975; Berko et al., 1975; de la Beaujardière et al., 1977; Theile and Whilhelm, 1980]. More recently, Burke [1981]] and Burke et al. [1983], by using low-altitude measurements made onboard S3-2, have reported current intensities as high as 135 μA m⁻². This is not far from the ionospheric equivalent of the maximum current densities we have observed at the equator.

The horizontal extension of intense arcs, usually associated with strong upwards current, is in general much larger than the dimensions that are quoted here (R \simeq 1 - 40 km at ionospheric level). However, structures localized both in latitude and longitude have been evidenced recently. By using the data of the Scandinavian chain of magnetometers and my modelling the conductivities and current systems, Baumjohann et al. [1981] have deduced the existence of strong upward currents ($8~\mu A~m^2$) near the westward boarder of the travelling surge during local auroral break-ups. Their size was of the order of the grid that they used (50 x 50 km²). A similar conclusion was arrived at by Bösinger et al. [1981], who indeed have also observed that these events were associated with strong SIP's. Mauk and Parks [1981] and Mauk et al. [1981], by using a new balloon-borne X ray imaging technique, have found structures whose size at the ionospheric level was within their resolution limit (20x20 km²) during a major break-up event. These structures were

associated with a softer spectrum of the precipitating electrons. Burke [1981] and Burke et al. [1983] have reported size structures of the order of 2 km.

As far as velocities are concerned, typical velocities of ~ 0.3 to 1.6 km s⁻¹ have been reported for the poleward motion of an arc [Nielsen and Greenwald, 1978]. Yet longitudinal velocities, of



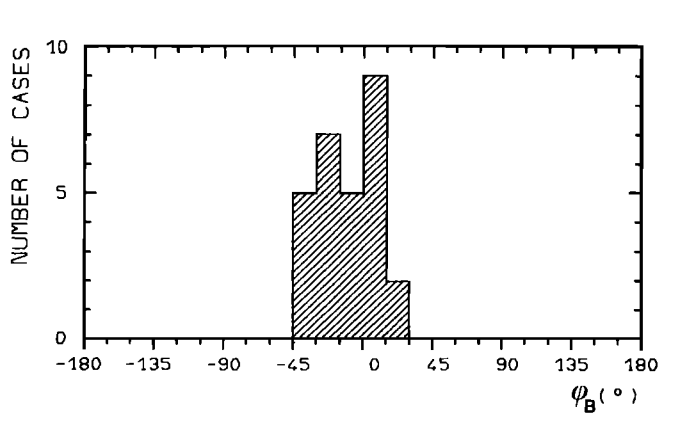


Fig. 18. Histogram of the direction of the dc magnetic field B for cases for which $|\Delta \varphi| \leq 40^\circ$. $\theta_B = (\underline{H}, \underline{B})$ and $\theta_B = (V, B_1)$ is measured in the V, D plane positively counterclockwise as seen from the North Pole. The average value of θ_B is 38°, showing that in the majority of cases \underline{B} has not recovered its dipolar configuration ($\overline{\theta}_B$ as almost always equal to $\simeq 0^\circ$ and not to $\simeq 180^\circ$, showing that \underline{B} is pointing toward the tail, i.e., that GEOS is almost always south of the neutral sheet.

the surge, for instance, may reach values as high as 2.5 km s [Akasofu et al., 1965], and even much higher velocities (up to 35 km s) have been reported [Bösinger et al., 1981; Ullaland et al., 1981]. It must be noted that such velocities seldom agree in direction (or intensity) with the one that can be deduced from the E x B drift, when electric field measurements are available either from rocket flights or from ground observations [Nielsen and Greenwald, 1978; Yamagashi et al., 1981]. This is partly due to the very intricate structure of the dc electric field in the vicinity of a surge [Horwitz et al., 1978] or more generally in the Harang discontinuity region where both the eastward and westward electrojets merge together [e.g., Kamide, 1978]. Akasofu [1979] has also argued that there was no reason why the ionospheric velocities should match the equatorial ones.

5.4. Experimental Difficulties

From the above brief review of the measurements made in the vicinity of bright auroral arcs, it appears that the ionospheric values of the current structures that we deduce from our equatorial measurements are in reasonable agreement with existing observations. The existence of localized field-aligned structures, that intensify at substorm onsets, have been emphasized by many observers [e.g., Kamide and Akasofu, 1975; Pytte et al., 1976; Meng et al., 1978]. But their characteristics are difficult to measure: their magnetic signature on the ground is just due to their associated Hall currents [Fukushima, 1971, 1976] and can be hidden by the magnetic effect of the simultaneous ionospheric westward electrojet. Precise measurements may disentangle the two signatures on some occasions [Opgenoorth et al., 1980; Inhester et al., 1981].

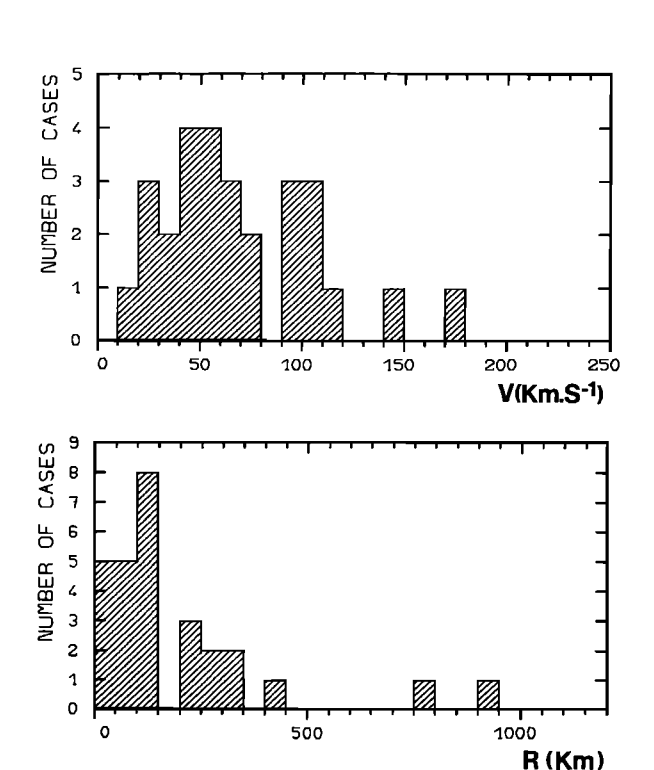
Above the ionosphere these currents are detectable in principle but if they are localized they

Table 1. Current Characteristics

	Minimum	Maximum	Average
Equatorial Values			
Radius R _e , km *	20	900	215
Density J _e , μA/m²	6x10 ⁻³	0.3	8x10 ⁻²
Velocity v _e , km/s	15	170	70
Ionospheric Values			
Radius R _i , km	1	40	10
Density Ĵ μA/m²	3	150	40
Velocity, v _i , km/s	1	10	4.5

In the above table, only the 28 events for which $\Delta \varphi = |-\underline{v}_s, \underline{v}_E| \le 40^\circ$ have been included in this analysis.

*For long lasting signatures, the cross section in the spin plane of the current structure is not necessarily circular (at least this cannot be proven without ambiguity). In these cases R is the size of the structure in the direction of its motion.



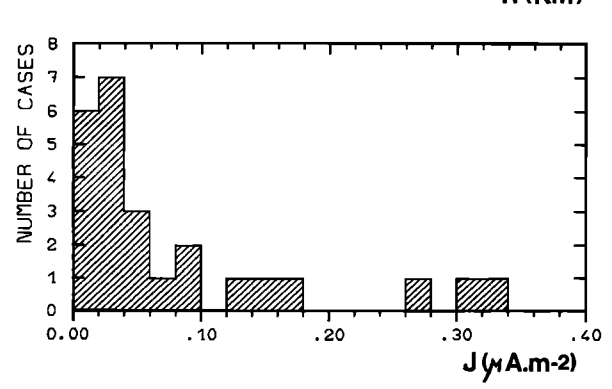


Fig. 19. Histograms of the current characteristics for events with $|\Delta \varphi| \le 40^\circ$. From top to bottom: velocity, radius, and current density.

may well be missed by orbiting satellites. Their size is much smaller than the size of the more or less permanent double sheet polar current system and even smaller than the small-scale disturbances (= 80 km) detected by TRIAD [Saflekos et al., 1978]. Even if a spacecraft was passing in their vicinity (a = 40 km) at the right time, their magnetic signature would be weak (25 to 250nT) for the quoted values of (JR). At larger distances (a \simeq 400 km) the magnetic amplitude (2.5 - 25 nT) falls near or below the resolution level ($\simeq 15$ nT) of the TRIAD satellite. MAGSAT, whose resolution is better ($\simeq 2nT$), will probably give more precise measurements. Indeed it seems that localized FACT structures have been detected in the vicinity of the Harang discontinuity (T.Iijima, private communication, 1981).

The use of ac antennas which are more sensitive to dB/dt than dc sensors, may help detecting these structures. Indeed Berko et al. [1975], who have used OGO 4 search coils and who have interpreted their results with a model similar to the one that is presented in this paper, were able to

detect some of these high intensity events. However, at low altitudes, the spacecraft velocity is equal to or larger than the velocity of the tube. Therefore, it is difficult to disentangle spatial effects from temporal ones. This is not the case for experiments performed at a few earth radii in the equatorial region since the spacecraft velocity is always negligible with respect to the structure velocity.

6. Interpretation of the Results

In this section we will consider the possible interpretation of our results in the frame of the current disruption model of substorm onsets and in terms of the theory of kinetic Alfven waves. We will also discuss the problems of the current limitation and of the origin of the electric field.

6.1. The Current Disruption Model

One of the favored theory for explaining field-aligned current enhancements is the diversion theory in which a fraction of the dawn to dusk neutral sheet current is suddenly diverted toward the ionosphere [Atkinson, 1967a, b; Boström, 1972; Akasofu, 1972, 1977, 1979]. Hasegawa and Sato [1979] and Sato and lijima [1979] have elaborated on this theory; they have shown that strong parallel currents occur in regions where vorticities in the plasma flow are present, as in the case at the boundary between a corotating plasma and a newly injected plasmasheet plasma. The fact that the strongest SIP's, i.e., those that are observed at substorm onsets, are localized in the midnight sector (see Figure 17) is an argument in favor of this theory. The estimated value of the diverted current (a few 10-8A m⁻²) is also in good agreement with the measured values.

A theory taking into account the ionospheric conductivity and the feedback mechanism that is introduced by the precipitating electrons has also been worked out by Atkinson [1979], who estimated the azimuthal velocity of the diversion slot to be of the order of 5 km s $^{-1}$ at the ionospheric level. This value agrees well with the ones we have deduced from our measurements.

However, these theories were mainly aimed at the interpretation of large scale structures. They do not contain any physical argument which could justify the smallness of the observed structures.

6.2. Kinetic Alfven Waves

When considering structures of a few ion gyroradii it is tempting to think of kinetic Alfven waves (KAW), which are potentially efficient processes of transmitting to the ionosphere any perturbation of the convection pattern occurring in the equatorial plasmasheet [Hasegawa, 1976; Mallinckrodt and Carlson, 1978; Goertz and Boswell, 1979]. Localized changes may indeed lead to kinetic effects provided that their spatial scales in the direction perpendicular to the magnetic field is of the order of the plasma inertial length [Goertz, 1981] or to the ion Larmor radius. As a consequence KAW's have a small but finite parallel electric field which might accelerate electrons. However, the overall effect of this E // does not necessarily lead to an important electron acceleration; this is why Lysak and Carlson [1981] have argued that the

microscopic turbulence associated with the KAW might lead to its damping. Later, Lysak and Dum [1982] proposed that this turbulent layer, in addition to modifying KAW reflexion, also leads to a partial current interruption through anomalous resistivity. They also evaluated the subsequent electron acceleration.

Since, for most of the studied examples, δ E/ δ B (where δ B is the amplitude of the magnetic signature) is of the order of the Alfven velocity, it is tempting to conclude that our observations are nothing but the signatures of KAW's. We have carefully examined the possible links between our data and the above theories. Examining Figures 6, 7a, 7b, 8a, and 8b, we find that over five events randomly selected there is only one for which δ E and δ B correlate in time. For the four other cases the δ E spikes are observed significantly earlier than the magnetic signature and they do not correlate.

Besides, the constancy of the E field direction during the whole event (see, e.g. Figures 7 and 8) is not compatible with the hypothesis of an Alfven wave for which the electric field should present a left-handed rotating pattern [Goertz, 1981]. It is worth mentioning that Burke et al. [1981] have also noticed the absence of change of direction of the electric field during the events that they reported. We thus conclude that the KAW model by itself cannot provide a fully satisfying explanation of our data; instead these are consistent with current structures moving past the spacecraft, as a response to an E field impulse.

6.3. <u>Current Limitations</u>

The ionospheric equivalent of the maximum current densities which we observe in the equatorial region (see Table 1) is of the same order of magnitude as the ones that were observed on some occasions at low altitudes [Berko et al., 1975; Burke, 1981; Burke et al., 1983] for localized structures. These values ($100 \mu A m^2$) far exceed the critical value ($\approx 2\text{-}10 \mu A m^2$) above which Kindel and Kennel [1971] have predicted that currents would become unstable with respect to ion-cyclotron or ion-acoustic waves. The fact that such high values are seldom observed at low altitudes may be a proof that the Kindel and Kennel's mechanism operates at low ($\simeq 1000$ km) altitudes. However, the extrapolation to higher altitudes may not be valid since we often observe in the equatorial region current densities much higher than the ones which can be deduced from Kindel and Kennel's theory (4 x 10 - 2 x 10 A m⁻²). Still we are faced with the problem of finding an explanation to the fact that in the equatorial region currents seldom exceed values of 10 A m 2 (Figure 19). A tentative explanation is given below.

Let B be the dc magnetic field and B φ the azimuthal z field generated by the FACT at its border. The Kruskal-Schwartzchild stability limit [Kruskal and Schwartzchild, 1954; Shafranov, 1956], which is defined as the maximum current that can flow along a field line before it becomes disrupted by its helical motion is given by

$$B_{\varphi}/B_{z} = 2\pi R/\Omega \tag{4}$$

where R is the radius of the current tube and $\hat{\mathbf{L}}$ is the parallel wavelength of the instability

that, for the first mode, can be taken equal to the characteristic length of the current tube.

Since $B\varphi = \mu JR/2$ and taking for L twice the length of inhomogeneity of a dipolar field ($L = 2\sqrt{2}LR_e/3$ where $R_E = 6400$ km and L is the McIlwain parameter) one obtains

$$J_{\text{max}} \simeq 2x10^{-4}/L^4 \quad \text{A m}^{-2}$$
 (5)

For L = 6.7, J $\simeq 10^{-7}~\rm A~m^{-2}$ which is not far from the maximum value observed onboard GEOS. Therefore we suggest that the Kruskal-Schwartzchild criterion defines the maximum current density in the equatorial region whereas the Kindel and Kennel mechanism may be a limiting process operating only at low altitudes ($\simeq 1000~\rm km$). Yet the instability might well account for the observed "turbulence" superimposed on the magnetic signatures. Note that a slightly modified version of the Kruskal-Schwartzchild criterion would lead to similar limitation of the current density inside current sheets.

6.4. Origin of the E Field

As shown in Figures 6, 7, and 8, electric field enhancements of a duration $\Delta\,t$ ranging from fractions of a minute to one minute have been observed at the time of SIP's. Typical length scales $\Delta\,t.V$ are then of the order of 10^3 km. Such a length scale represents a few gyroradii of 1 keV protons. Only the lower ion energies of the plasma will therefore have a bulk motion that is approximately \underline{ExB}/B^2 during the relatively short time of an electric field enhancement.

The somewhat surprising result v / |v| = -v / |v| at substorm onsets is nevertheless interesting, and it is worth repeating that this seems to be a reasonable way of determining the ambiguity in directions of current motions.

Another question of concern is the origin of this E field. Such a field cannot be reproduced through Faraday's law by the current displacement itself. Indeed it is easily found that a moving current can only generate an induction field parallel to itself. Therefore, if the current is field-aligned and if its intensity is not a function of the abscissa along the field line, there is no inductive field perpendicular to \underline{B} . If the current was not field-aligned, a simple order of magnitude computation shows that the induction field could not reach the observed values : considering the distance of closest approach a as a characteristic length, the relation $\nabla \times \underline{E} = -d\underline{B}/dt$ leads to $E \simeq a \Delta B/\tau$. Assuming a $\simeq 500$ km, $\Delta B \simeq 5$ nT, and $\tau \simeq 5$ s, one gets $E \approx 0.5$ mV·m⁻¹, which is much smaller than the observed values. In addition observations show that the large E spikes are not in general coincident in time with the magnetic signature. Therefore the measured electric field does not seem to be associated with the space charge set up by the field-aligned current [e.g., Goertz and Boswell, 1979]. The situation is different from the one encountered at ionospheric altitude where such space-charge generated electric fields seem to have been observed in conjunction with intense field-aligned currents [Burke et al., 1983].

The events being mostly observed at times of plasma injection, polarization electric fields associated with plasma boundaries may also well be invoked. In fact, if actually the current is divert-

ed from the neutral sheet, stresses on magnetic field lines may be at the origin of the tube displacement, as in flux transfer events, and again it is not obvious how electrostatic fields are generated in such structures.

7. Conclusion

By making a careful analysis of ULF signals detected onboard GEOS 2 during substorm events, we obtained results which may be summarized as follows:

- 1. There is a definite correlation between magnetospheric substorms and short irregular pulsations. SIP's detected in the outer magnetosphere onboard spacecraft principally occur in conjunction with abrupt changes of the dc magnetic field from a taillike to a more dipolar configuration. These changes may be considered as defining the substorm onsets at GEOS and at its conjugate point. However, SIP's may be observed at other periods during substorms.
- 2. The wave form of a large fraction of SIP's may be interpreted as the signature of a current structure passing by the spacecraft with a high velocity. When the magnetic turbulence associated with these currents is too strong, this signature cannot be derived with confidence.
- 3. When the experimental conditions are favorable (i.e., when the current is moving fast so that the magnetic signature lasts less than 2 s) it is possible to show that the currents are field-aligned. 4. In 40% of cases so far analyzed, the direction of the tube displacement (as deduced from its magnetic signatures on orthogonal antonnas) agrees within $\simeq 20^{\circ}$ with the one which is computed from the simultaneous measurement of the quasistatic electric field (v = ExB/B²). When the comparison is restricted to SIP's associated with substorm onsets (as defined above) this percentage raises to 64° (9 cases out of 14) and reach 100% for an agreement between the two directions less than 40°.
- 5. If the assumption is made that for these cases the absolute value for the velocity of the structure is equal to the absolute value of the drift velocity v, the other current parameters (size, density) can be computed (Table 1). Average values for the current parameters, as measured in the equatorial region, are $R\approx 215$ km, $J\approx 8\times 10^{-8}$ A m⁻², and $v\approx 70$ km s⁻¹.
- 6. A transposition of these characteristics to ionospheric levels gives figures that are in reasonable agreement with the typical values recently found for localized current structures associated with break up events.
- 7. Magnetic signatures of localized structures tend to occur significantly after strong spikes in the quasi dc electric field. This lack of simultaneity seems to argue against an explanation based upon kinetic Alfven waves. Instead, observed signatures are consistent with field-aligned current structures (be it tubes or not) moving fast as a response to a more or less spatially localized impulse in the E field.
- 8. Current structures detected precisely at "substorm onsets" move preferentially in an azimuthal direction (in agreement with the diversion current theory). A definite conclusion cannot be reached for those detected during the other substorm phases because of the observed differences

between the displacement directions deduced from the magnetic signatures and the $E \times B$ direction. 9. The maximum current density that is observed $(J \approx 3 \times 10^{-7} \text{ A m}^{-2})$ in the equatorial region, which corresponds to $J \approx 1.5 \times 10^{-7} \text{ A m}^{-2}$ at ionospheric level) is well interpreted in terms of MHD stability of helicoidal currents (Kruskal- Schwartzchield criterion).

The behavior of medium or low energy particles associated with such structures has not yet been analyzed. This study, which requires high time resolution particle data will be a task for a future work. Similarly, a detailed comparison with high resolution magnetometer data (S-331) has not been made so far. Such a comparison would greatly help determining the geometry of current signatures of duration longer than 2 s.

Nevertheless, it is clear from this study that localized, short-lived and probably field-aligned structures are created during substorms and that they could well play a fundamental role in their triggering. It should also be kept in mind that the magnetic signatures of these fastly moving currents are often accompanied by intense turbulent magnetic and electric fields in the range 1-10 Hz. Further studies are required in order to determine the role of these fields in connection with SIP's.

Acknowledgments. The ULF experiment onboard GEOS is part of a cooperative experiment conceived and operated by five European institutes. We thank the scientists, engineers, and technicians involved in this cooperation for their contribution to this successful experiment. The ESA Operation Center at Darmstadt (Germany) and the Division of Mathematics at CNES in Toulouse (France) must also be thanked for their efficiency in the routine data handling and processing. One of us (R.G.) is indebted to T. Iijima, N. Fukushima (University of Tokyo), Y. Kamide (Kyoto Sangyo University), and T. Sato (University of Hiroshima) for discussions he had with them on substorm phenomena and field-aligned current systems during his three-months stay at the National Institute of Polar Research. T. Nagata, Director of NIPR, and staff members of this Institute are gratefully acknowledged for their kind hospitality during this stay. We also thank both referees for their constructive criticisms and their careful reading of this paper

References

- Akasofu, S.-I., Magnetospheric substorms: A model, in Solar Terrestrial Physics, Leningrad 1970, vol. 3, edited by E.R. Dyer and J.G. Roederer, pp. 131-155, D. Reidel, Hingham, Mass., 1972.
- Akasofu, S.-I., Physics of Magnetospheric Substorms, D. Reidel, Hingham, Mass., 1977.
- Akasofu, S.-I., What is a magnetospheric substorm?, in <u>Dynamics of the Magnetosphere</u>, edited by S.-I. Akasofu, pp. 447-460, D. Reidel, Hingham, Mass., 1979.
- Akasofu, S.-I., D. S. Kimball, and D. J. Meng, Dynamics of the aurora, 2, Westward travelling surges, J. Atmos. Terr. Phys., 27, 173-187, 1965.
- Atkinson, G., An approximate flow equation for geomagnetic flux tubes and its application to polar substorms, J. Geophys. Res., 72, 5373-5382, 1967a.
- Atkinson, G., The current system of geomagnetic

- bays, J. Geophys. Res., 72, 6063-6067, 1967b. Atkinson, G., The expansive phase of the magnetospheric substorms, in <u>Dynamics of the Magnetosphere</u>, edited by S.-I. Akasofu, pp. 461-481, D. Reidel, Hingham Press, Mass., 1979.
- Aubry, M. P., M. G. Kivelson, R. L. McPherron, and C. T. Russell, Outer magnetosphere near midnight at quiet and disturbed times, J. Geophys. Res., 77, 5487-5502, 1972.
- Baumjohann, W., R. J. Pellinen, H. J. Opgenoorth, and E. Nielsen, Joint two-dimensional observations of ground magnetic and ionospheric electric fields associated with auroral zone currents: Current systems associated with local auroral break-ups, Planet. Space Sci., 29, 431-477, 1981.
- Berko, F. W., R. A. Hoffmann, R. K. Burton, and R. E. Holzer, Simultaneous particle and field observations of field-aligned currents, <u>J. Geophys.</u> Res., 80, 37-46, 1975.
- Res., 80, 37-46, 1975.

 Bösinger, T., K. Alanko, J. Kangas, H. Opgenoorth, and W. Baumjohann, Correlations between PiB type magnetic micropulsations, auroras and equivalent current structures during two isolated substorms, J. Atmos. Terr. Phys., 43, 933-945, 1981.
- Boström, R., Magnetosphere-ionosphere coupling, in <u>Critical Problems of Magnetospheric Physics</u>, edited by E. R. Dyer, pp. 139-156, National Academy of Science, Washington, D.C., 1972.
- Burke, W. J., Electric fields, Birkeland currents and electron precipitation in the vicinity of discrete auroral arcs, in Physics of the Auroral Arc Formation, Geophys. Monogr. Ser., vol. 25, edited by S.-I. Akasofu and J. R. Kan, pp. 164-172, AGU, Washington, D. C., 1981.
- Burke, W. J., M. Silevitch, and D. A. Hardy, Observations of small-scale auroral vortices by the S3-2 satellite, J. Geophys. Res., 88, 3127-3137, 1983.
- Casserly, R. T., Jr., and P. A. Cloutier, Rocket-based magnetic observations of auroral Birkeland currents in association with a structured auroral arc. J. Geophys. Res., 80, 2165-2168, 1975.
- arc, <u>J. Geophys. Res.</u>, <u>80</u>, 2165-2168, 1975. de la Beaujardière, O., R. Vondrak, and M. Baron, Radar observations of electric fields and currents associated with auroral arcs, <u>J. Geophys. Res.</u>, <u>82</u>, 5051-5062, 1977.
- Fairfield, D. H., Magnetic field signatures of substorms on high-latitude field lines in the night-time magnetosphere, <u>J. Geophys. Res.</u>, 78, 1553-1562, 1973.
- Frank, L. A., R. L. McPherron, R. J. DeCoster, B. G. Burek, K. L. Ackerson, and C. T. Russell, Field-aligned currents in the earth's magnetotail, J. Geophys. Res., 86, 687-700, 1981.
- Fukushima, H., Electric current systems for polar substorms and their magnetic effects below and above the ionosphere, Radio Sci., 6, 269-275, 1971.
- Fukushima, H., Generalized theorem for non ground magnetic effects of vertical currants connected with Pedersen currents in the uniform-conductivity ionosphere, Rep. Ionos. Space Res. Jpn., 30, 35-40, 1976.
- Gendrin, R., Substorm aspects of magnetic pulsations, Space Sci. Rev., 11, 54-130, 1970.
- Goertz, C. K., Discrete break-up arcs and kinetic Alfven waves, in <u>Physics of the Auroral Arc Formation</u>, <u>Geophys. Monogr. Ser.</u>, vol. 25, edited by S.-I. Akasofu and J. R. Kan, pp.

- 451-455, AGU, Washington, D. C., 1981.
- Goertz, C. K., and R. W. Boswell, Magnetosphereionosphere coupling, <u>J. Geophys. Res.</u>, <u>84</u>, 7239-7246, 1979.
- Hasegawa, A., Particle acceleration by MHD surface wave and formation of aurora, <u>J. Geophys. Res.</u>, <u>81</u>, 5083-5090, 1976.
- Hasegawa, A., and T. Sato, Generation of fieldaligned current during substorm, in <u>Dynamic</u> of the <u>Magnetosphere</u>, edited by S.-I. Akasofu, pp. 529-542. D. Reidel, Hingham, Mass., 1979.
- pp. 529-542, D. Reidel, Hingham, Mass., 1979. Horwitz, J. L., J. R. Doupnik, and P. M. Banks, Chatanika radar observations of the latitudinal distributions of auroral zone electric fields, conductivities and currents, J. Geophys. Res., 83, 1463-1481, 1978.
- Iijima, T., Signatures of field-aligned currents at geostationary satellite ATS-1 and a refined three-dimensional substorm current system, Rep. Ionos. Space Res. Jpn., 28, 173-177, 1974.
- Rep. Ionos. Space Res. Jpn., 28, 173-177, 1974. Iijima, T., and T. A. Poternra, Large-scale characteristics of field-aligned currents associated with substorms, J. Geophys. Res., 83, 599-615, 1978.
- substorms, J. Geophys. Res., 83, 599-615, 1978. Inhester, B., W. Baumjohann, R. A. Greenwald, and E. Nielsen, Joint two-dimensional observations of ground magnetic and ionospheric electric fields associated with auroral zone currents, J. Geophys., 49, 155-162, 1981.
- Kamide, Y., On current continuity at the Harang discontinuity, Planet. Space Sci., 26, 237-244, 1978.
- Kamide, Y., Recent progress in observational studies of electric fields and currents in the polar ionosphere: a review, Antarctic Record Nr. 63, National Institute of Polar Research, Tokyo, 61-231, 1979.
- Kamide, Y., and S.-I. Akasofu, The auroral electrojet and global auroral features, <u>J. Geophys. Res.,</u> 80, 3585-3602, 1975.
- Kindel, J. M.., and C. F. Kennel, Topside current instabilities, <u>J. Geophys. Res.</u>, <u>76</u>, 3055-3078, 1971.
- Knott, K., Payload of the GEOS scientific geostationary satellite, ESA Sci. Techn. Rev., 1, 173-196, 1975.
- Kruskal, M., and M. Schwartzchild, Some instabilities of a completely ionized plasma, <u>Proc. R. Soc. London</u>, A 223, 348, 1954.
- Lycak, R. L., and C. W. Carlson, The effect of microscopic turbulence on magnetosphere-ionosphere coupling, Geophys. Res. Lett., 8, 269-272, 1981.
- Lysak, R. L., and C. T. Dum, Dynamics of magnetosphere-ionosphere coupling including turbulent transport, J. Geophys. Res., 88, 365-380, 1983. Mallinkrodt, A. J., and C. W. Carlson, Relations
- between transverse electric fields and field-aligned currents, <u>J. Geophys. Res.</u>, <u>83</u>, 1426-1432, 1978.
- Mauk, B. H., and C. K. Parks, X ray images of an auroral break-up in Physics of the Auroral Arc Formation, Geophys. Monogr. Ser., vol. 25, edited by S.-I. Akasofu and J. R. Kan, AGU, Washington, D. C., 1981.
- Mauk, B. H., J. Chin, and G. K. Parks, Auroral X ray images, <u>J. Geophys. Res.</u>, <u>86</u>, 6827-6835, 1981.
- McPherron, R. L., Magnetospheric substorms, Rev. Geophys. Space Phys., 17, 657-681, 1979. McPherron, R. L., and J. N. Barfield, A seasonal

change in the effects of field-aligned currents

- at synchronous orbit, J. Geophys. Res., 85, 6746-6747, 1980.
- McPherron, R. L., P. J. Coleman Jr., and R. C. Snare, ATS 6 UCLA fluxgate magnetometer, IEEE Trans. Aerosp. Electron. Syst., AES-11, 1110-1117, 19/5.
- Meng., C. I., A. L. Snyder, Jr., and H. W. Kroehl, Observations of auroral westward travelling surges and electron precipitations, <u>J. Geophys.</u> <u>Res.</u>, <u>83</u>, 575-579, 1978.
- Mozer, F. S., C. A. Catell, M. Temerin, R. B. Torbert, S. von Glinski, M. Woldorfi, and J. Wygant, The dc and ac electric field, plasma density and field-aligned current experiments on the S3-3 satellite, J. Geophys. Res., 84, 5875-5884, 1979.
- Nielsen, E., and R. A. Greenwald, Variations in ionospheric currents and electric fields in association with absorption spikes during the substorm expansion phase, <u>J. Geophys. Res.</u>, 83, 5645-5654, 1978.
- 83, 5645-5654, 1978.

 Opgenoorth, H. J., R. J. Pellinen, H. Maurer, F. Küppers, W. J. Heikkila, K. U. Kaila, and P. Tanskanen, Ground-based observatins of an onset of localized field-aligned currents during auroral break-up around magnetic midnight, J. Geophys. Res., 48, 101-115, 1980.
- night, J. Geophys. Res., 48, 101-115, 1980. Pedersen, A., R. Grard, K. Knott, D. Jones, and A. Gonfalone, Measurements of quasi-static electric fields between 3 and 7 earth radii on GEOS 1, Space Sci. Rev., 22, 333-346, 1978.
- Perraut, S., A. Roux, P. Robert, R. Gendrin, J. A. Sauvaud, J. M. Bosqued, G. Kremser, and A. Korth, A systematic study of ULF waves above F_H+ from GEOS I and 2 measurements and their relationships with proton ring distributions, J. Geophys. Res., 87, 6219-6236, 1982
- J. Geophys. Res., 87, 6219-6236, 1982.

 Pytte, T., H. Trefall, G. Kremser, L. Jalonen, and W. Riedler, On the morphology of energetic (> 30 keV) electron precipitation during the growth phase of magnetospheric substorms, J. Atmos. Terr. Phys., 38, 739-755, 1976.
- Potemra, T. A., Current systems in the earth's magnetosphere, Rev. Geophys. Space Phys., 17, 640-656, 1979.
- Robert, P., K. Kodera, S. Perraut, R. Gendrin, and C. de Villedary, Amplitude et polarisation des ondes UBF détectées à bord du satellite GEOS 1: Méthodes d'analyse, problèmes rencontrés et solutions pratiques, Ann. Telecom., 34, 179-186, 1979.
- Rostoker, G., Recent advances in the study of electric and magnetic fields in the ionosphere and magnetosphere, J. Geomagn. Geoelectr., 32, 431-470, 1980.
- Saflekos, N. A., T. A. Potemra, and T. Iijima, Small-scale transverse magnetic disturbances in the polar regions observed by TRIAD, <u>J. Geo-Phys. Res.</u>, 83, 1493-1502, 1978.
 Sato, T., and T. Iijima, Primary sources of large-
- Sato, T., and T. Iijima, Primary sources of largescale Birkeland currents, <u>Space Sci. Rev.</u>, 24, 347-366, 1979.
- 347-366, 1979.

 Shafranov, V. D., The stability of a cylindrical gaseous conductor in a magnetic field, Soviet J. At. Energy Engl. Transl., 1, 709, 1956.

 Shepherd, G. G., R. Boström, H. Derblom, C. G.
- Falthammar, R. Gendrin, K. Kaila, A. Korth, A. Pedersen, R. Pellinen, and G. L. Wrenn, Plasma and field signatures of a poleward propagating auroral precipitation observed

- at the foot of the GEOS ? field line, <u>J. Geophys.</u> Res., <u>85</u>, 4587-4601, 1980.
- Stern, D. P., The electric field and global electrodynamics of the magnetosphere, Rev. Geophys. Space Phys., 17, 626-640, 1979.
- S-300 Experimenters, Measurements of electric and magnetic wave field and cold plasma parameters onboard GEOS 1: Preliminary results, Planet. Space Sci., 27, 317-339, 1979.
- Theile, B., and K. Wilhelm, Field-aligned currents above an auroral arc, <u>Planet. Space Sci.</u>, 28, 351-355, 1980.
- Ullaland, S., J. Bjordal, L. P. Block, K. Bronstadt, I. B. Iversen, J. Kangas, A. Korth, G. Kremser, M. M. Madsen, T. Moe, W. Riedler, J. Stadnes, T. Tanskanen, and K. M. Torkar, Triggering of magnetospheric substorm by a sudden commencement of a geomagnetic storm observed by the X-ray experiment onboard SBARMO 79 and the charged particle spectrometer on GEOS 2, in Advances in Space Res., Vol. 1, edited by K. Knott, pp. 273-278, Pergamon, New-York, 1981.
- Yamagishi, D. T., M. Eijiri, T. Hirasawa, K. Tsuruda, I. Kimura, and A. Nishida, The results of auroral sounding with S-310-JA-4 rocket: Electric field, particles and waves, in <u>Proceedings of the Third Symposium on Coordinated Observa-</u>

- tions of the Ionosphere and the Magnetosphere in Polar Regions, edited by T. Nagata, pp. 335-354, National Institute of Polar Research, Tokyo, 1981.
- Young, D. T., S. Perraut, A. Roux, C. de Villedary, R. Gendrin, A. Korth, G. Kremser, and D. Jones, Wave-particle interactions near observed on GEOS 1 and 2: 1, Propagation of ion cyclotron waves in He⁺-rich plasma, J. Geophys. Res., 86, 6755-6772, 1981.
- Zmuda, A. J., J. C. Armstrong, and F. T. Heuring, Characteristics of transverse magnetic disturbances observed at 1100 km in the auroral oval, J. Geophys. Res., 75, 4757-4762, 1970.
- R. Gendrin, S. Perraut, P. Robert, and A. Roux, Centre de Recherches en Physique de l'Environnement Terrestre et Planétaire,
- Centre National d'Etudes des Télécommunications 92131 Issy-les-Moulineaux, France.
- A. Pedersen, Space Science Department, European Space Research and Technology Center 2200 AG-Noordwijk, The Netherlands.

(Received August 26, 1982; revised November 7, 1983; accepted November 8, 1983.)